

Flavour Violation in Gauge-Mediated Supersymmetry Breaking Models: Experimental Constraints and Phenomenology at the LHC

Benjamin Fuks

*Physikalisches Institut, Albert-Ludwigs-Universität Freiburg,
Hermann-Herder-Straße 3, D-79106 Freiburg im Breisgau, Germany*

Björn Herrmann and Michael Klasen*

*Laboratoire de Physique Subatomique et de Cosmologie,
Université Joseph Fourier/CNRS-IN2P3/INPG, 53 Avenue des Martyrs, F-38026 Grenoble, France*

(Dated: October 24, 2018)

We present an extensive analysis of gauge-mediated supersymmetry breaking models with minimal and non-minimal flavour violation. We first demonstrate that low-energy, precision electroweak, and cosmological constraints exclude large “collider-friendly” regions of the minimal parameter space. We then discuss various possibilities how flavour violation, although naturally suppressed, may still occur in gauge-mediation models. The introduction of non-minimal flavour violation at the electroweak scale is shown to relax the stringent experimental constraints, so that benchmark points, that are also cosmologically viable, can be defined and their phenomenology, i.e. squark and gaugino production cross sections with flavour violation, at the LHC can be studied.

I. INTRODUCTION

Weak scale supersymmetry (SUSY) remains a both theoretically and phenomenologically attractive extension of the Standard Model (SM) of particle physics [1, 2]. Apart from linking bosons with fermions and unifying internal and external (space-time) symmetries, SUSY allows for a stabilization of the gap between the Planck and the electroweak scale and for gauge coupling unification at high energies. It appears naturally in string theories, includes gravity, and contains a stable lightest SUSY particle (LSP) as a dark matter candidate. Spin partners of the SM particles have not yet been observed, and in order to remain a viable solution to the hierarchy problem, SUSY must be broken at low energy via soft mass terms in the Lagrangian. As a consequence, the SUSY particles must be massive in comparison to their SM counterparts, and the Tevatron and the LHC will perform a conclusive search covering a wide range of masses up to the TeV scale. After the discovery of SUSY particles, the revelation of the underlying SUSY-breaking mechanism will be one of the key challenges in the experimental high-energy physics program.

In gauge-mediated supersymmetry-breaking (GMSB) models, SUSY is broken in a secluded sector at a scale $\langle F \rangle$ related to the gravitino mass by $m_{\tilde{G}} = \langle F \rangle / (\sqrt{3} M_P)$, where M_P is the reduced Planck mass. The breaking is mediated to the visible sector of squarks, sleptons, gauginos and gluinos through a gauge-singlet chiral superfield S and n_q quark-like and n_l lepton-like messenger fields [3–6]. The superfield S is characterized by its scalar and auxiliary components, which overlap with the gravitino and acquire vacuum expectation values $\langle S \rangle$ and $\langle F_S \rangle$, respectively. Yukawa couplings of the messengers to the superfield S then induce masses of order $M_{\text{mes}} \simeq \langle S \rangle$ for the messengers. Gauginos and sfermions acquire masses through ordinary gauge interactions with messengers through one- and two-loop self-energy diagrams, respectively. In these scenarios, the lightest SUSY particle is always the gravitino, which is thus a natural candidate for the dark matter in our Universe. Besides M_{mes} , n_q , and n_l , minimal GMSB scenarios are determined by the ratio of the two Higgs vacuum expectation values, $\tan \beta$, the sign of the off-diagonal Higgs mass-parameter μ , and by the auxiliary vacuum expectation value $\langle F_S \rangle$. The latter is related to the mass splitting of the messenger fields and is considerably smaller than both the squared mass scale of the messenger fields, $\langle S \rangle^2$, and the fundamental SUSY-breaking scale, $\langle F \rangle$. It is usually re-expressed in terms of an effective SUSY-breaking scale, $\Lambda = \langle F_S \rangle / \langle S \rangle$. An additional free parameter is the gravitino mass, $m_{\tilde{G}}$, which is, however, constrained by the fact that the gravitino relic density $\Omega_{\tilde{G}} h^2$ has to agree with the current WMAP limits and that the abundances of the light elements should be correctly described, i.e. the next-to-lightest SUSY particle (NLSP) must not decay too quickly.

GMSB is an attractive scenario regarding the so-called SUSY flavour problem. SUSY is usually broken within a few orders of magnitude of the weak scale, whereas the unrelated flavour-breaking scale can be chosen much higher. This avoids important flavour-violating terms in the SUSY-breaking Lagrangian and leads to approximately flavour-conserving mass matrices at the low-energy scale and good agreement with measurements of flavour-changing neutral

*klasens@lpsc.in2p3.fr

current observables. However, several possibilities reintroducing flavour-violating terms in the Minimal Supersymmetric Standard Model (MSSM) with GMSB have been pointed out [6–8]. For example, mixing between messenger and matter fields may lead to important flavour violations in the squark and slepton sectors.

In SUSY models with non-minimal flavour violation (NMFV), the flavour-violating off-diagonal terms Δ_{ij} of the squared sfermion mass matrices, where $i, j = L, R$ refer to the helicities of the (SM partners of the) sfermions, are conveniently considered as arbitrary parameters. Stringent experimental constraints are then imposed by precise measurements of $K^0 - \bar{K}^0$ and $B^0 - \bar{B}^0$ mixing, the first evidence of $D^0 - \bar{D}^0$ mixing, and rare decays [9–11]. The minimal GMSB model obviously relies on constrained minimal flavour violation (cMFV), where all the flavour-violating elements Δ_{ij} are neglected. Recently, possible effects of non-minimal flavour violation on the experimentally allowed minimal supergravity (mSUGRA) parameter space have been investigated, and all squark and gaugino production cross sections and decay widths have been recalculated including both helicity and flavour mixing in the squark sector [12]. The aim of this work is to extend this study to GMSB scenarios, to evaluate the experimental constraints, discuss the role of flavour violation, and make numerical predictions for squark- and gaugino-production cross sections at the LHC.

This paper is organized as follows: In Sec. II, we impose the current experimental constraints on the minimal GMSB models. We show that these scenarios are strongly disfavoured due to the very stringent constraint coming from the rare $b \rightarrow s\gamma$ decay. However, the latter can be relaxed by introducing NMFV in the squark sector, as shown in Sec. III, allowing us to define benchmark points for NMFV GMSB scenarios. Sec. IV is devoted to the discussion of cosmological implications on the gravitino mass in our scenarios. In Sec. V, we present numerical predictions for squark and gaugino hadroproduction cross sections at the LHC. Our conclusions are given in Sec. VI.

II. EXPERIMENTAL CONSTRAINTS ON GMSB MODELS WITH MINIMAL FLAVOUR VIOLATION

In the absence of experimental evidence for Supersymmetry, a large variety of data can be used to constrain the parameter space of the MSSM. Sparticle mass limits can be obtained from searches of charginos ($m_{\tilde{\chi}_1^\pm} \geq 150$ GeV from D0), neutralinos ($m_{\tilde{\chi}_1^0} \geq 93$ GeV in GMSB from the combination of LEP2 results), gluinos ($m_{\tilde{g}} \geq 195$ GeV from CDF), stops ($m_{\tilde{t}_1} \geq 95 \dots 96$ GeV for neutral- or charged-current decays from the combination of LEP2 results), other squarks ($m_{\tilde{q}} \geq 300$ GeV for gluinos of equal mass from CDF), and gravitinos ($m_{\tilde{G}} \geq 1.3 \cdot 10^{-5}$ eV for $m_{\tilde{q}} = m_{\tilde{g}} = 200$ GeV) at colliders [13, 14].

Cosmological, electroweak precision, and low energy observables can be used to put additional constraints on the SUSY parameter space. The theoretically robust inclusive branching ratio

$$\text{BR}(b \rightarrow s\gamma) = (3.55 \pm 0.26) \cdot 10^{-4}, \quad (1)$$

obtained from the combined measurements of BaBar, Belle, and CLEO [15], can be confronted to theoretical predictions including two-loop QCD and one-loop SUSY contributions [16, 17]. Squarks contribute here already at the one-loop level, as do the SM contributions. A second observable, sensitive to the squark-mass splitting within isospin doublets, is the electroweak ρ -parameter with

$$\Delta\rho = \frac{\Sigma_Z(0)}{m_Z^2} - \frac{\Sigma_W(0)}{m_W^2}, \quad (2)$$

where $m_{Z,W}$ and $\Sigma_{Z,W}(0)$ denote the Z - and W -boson masses and self-energies at zero momentum, respectively. New physics contributions are constrained by the latest combined electroweak precision measurements to $T = -0.13 \pm 0.11$ or

$$\Delta\rho = -\alpha T = (1.02 \pm 0.86) \cdot 10^{-3} \quad (3)$$

for $\alpha(m_Z) = 1/127.918$ [13]. This value is compared to theoretical calculations including SUSY two-loop corrections [18]. A third variable sensitive to new physics loop contributions is the anomalous magnetic moment of the muon, for which we require the SUSY contribution a_μ^{SUSY} , known up to the two-loop level [19, 20], to close the gap between recent BNL experimental data and the SM prediction [13],

$$\Delta a_\mu = (29.2 \pm 8.6) \cdot 10^{-10}. \quad (4)$$

Note that the one-loop SUSY contributions are approximatively given by [21]

$$a_\mu^{\text{SUSY}, 1\text{-loop}} \simeq 13 \cdot 10^{-10} \left(\frac{100 \text{ GeV}}{M_{\text{SUSY}}} \right)^2 \tan\beta \text{sgn}(\mu), \quad (5)$$

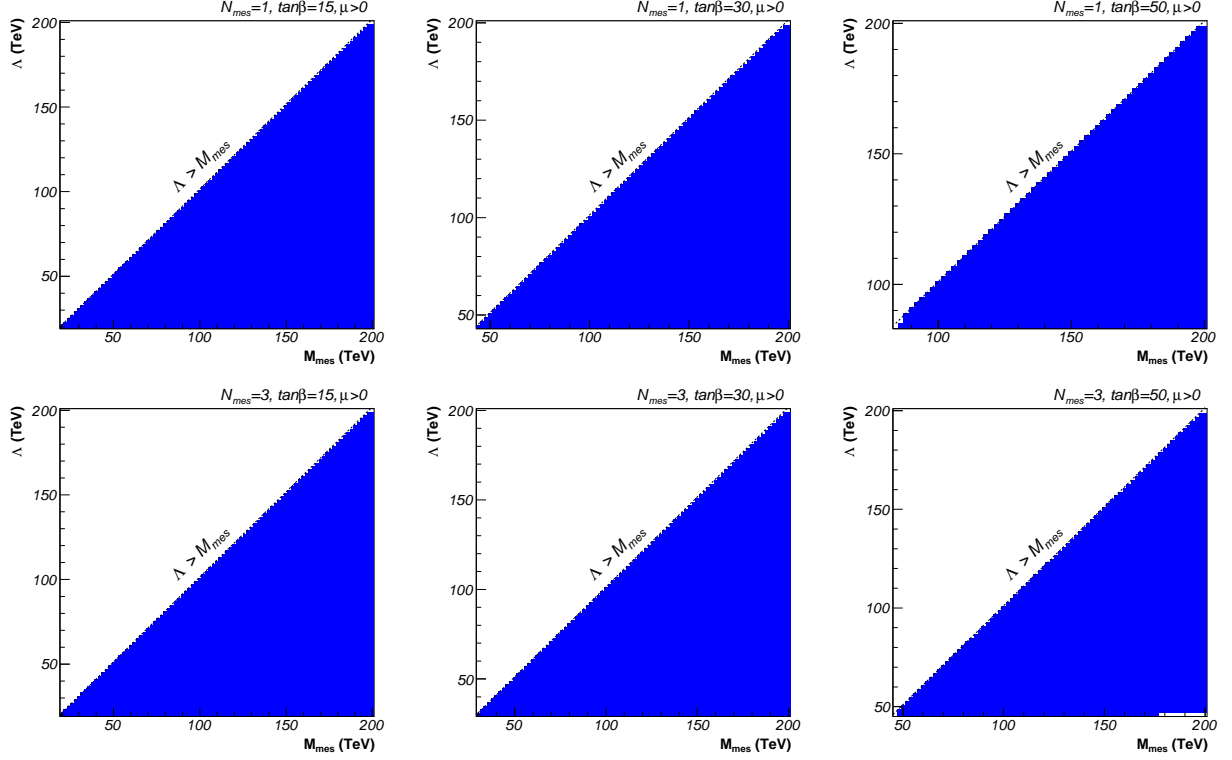


FIG. 1: The Λ – M_{mes} planes for $\mu > 0$ and different values of $\tan\beta$ and N_{mes} , assuming constrained minimal flavour violation. Dark (blue) regions are excluded by the constraint coming from the $b \rightarrow s\gamma$ branching ratio. The regions where $\Lambda > M_{\text{mes}}$ does not allow for physical solutions of the RGEs.

if the relevant SUSY particles have masses of the order of M_{SUSY} . As a consequence, negative values of μ then increase, not decrease, the disagreement between the experimental measurements and the theoretical value of a_μ , so that the region $\mu < 0$ is strongly disfavoured in all SUSY models. In addition, this region is also virtually excluded by the $b \rightarrow s\gamma$ constraint at the 2σ confidence level. We therefore restrict ourselves to positive values of μ throughout this analysis.

The above experimental limits are imposed at the 2σ confidence level on the minimal GMSB model with $\mu > 0$ and four free parameters Λ , M_{mes} , $N_{\text{mes}} \equiv n_q = n_l$, and $\tan\beta$. The renormalization group equations (RGEs) are solved numerically to two-loop order using the computer programme **SPheno** 2.2.3 [22], which computes the soft SUSY-breaking masses at the electroweak scale with the complete one-loop formulas, supplemented by two-loop contributions for the neutral Higgs bosons and the μ -parameter. We then diagonalize the mass matrices and compute the electroweak precision and low-energy observables with the computer programme **FeynHiggs** 2.6.4 [23]. For the SM input parameters, i.e. the masses and widths of the electroweak gauge bosons and quarks, the angles of the CKM-matrix and its CP -violating phase, and the Fermi coupling constant, we refer the reader to Ref. [13].

In Fig. 1, we show typical scans of the minimal GMSB parameter space in Λ and M_{mes} for different values of $\tan\beta$ (15, 30, and 50) and N_{mes} (1 and 3). The six panels reveal that these scenarios are strongly disfavoured by the measurements of the $b \rightarrow s\gamma$ branching ratio. In particular, the Snowmass benchmark points [24] SPS 7 ($\Lambda = 40$ TeV, $M_{\text{mes}} = 80$ TeV, $\tan\beta = 15$, $\mu > 0$, and $N_{\text{mes}} = 3$) and SPS 8 ($\Lambda = 100$ TeV, $M_{\text{mes}} = 200$ TeV, $\tan\beta = 15$, $\mu > 0$, and $N_{\text{mes}} = 1$) lead to values of $\text{BR}(b \rightarrow s\gamma) = 6.97 \cdot 10^{-4}$ and $6.77 \cdot 10^{-4}$, which are both excluded beyond the 5σ level, even if both of these points lie well within 2σ of the experimentally allowed range for the anomalous magnetic moment of the muon with $a_\mu^{\text{SUSY}} = 22.8 \cdot 10^{-10}$ and $a_\mu^{\text{SUSY}} = 16.31 \cdot 10^{-10}$. Note that the regions with $\Lambda > M_{\text{mes}}$ are theoretically excluded, since they do not allow for physical solutions of the RGEs.

Recently, a detailed study of electroweak precision observables, including scenarios with minimal GMSB, has been performed [25]. Scanning also over $\tan\beta$ and allowing for higher values of $N_{\text{mes}} \leq 8$, the authors show that experimentally favoured scenarios can be achieved at low messenger scales, which, however, implies a certain amount of fine tuning at the weak scale, e.g. in the Higgs sector. Note that for $N_{\text{mes}} \gtrsim 8$ problems with perturbativity of the gauge interactions arise at very high scales [6].

III. GMSB MODELS WITH NON-MINIMAL FLAVOUR VIOLATION

The minimal GMSB is known to suppress flavour-changing neutral currents as suggested by measurements and thus to avoid the SUSY “flavour problem”, which arises naturally in models where SUSY-breaking is mediated by gravity. Models beyond the minimal GMSB can, however, reintroduce flavour-breaking terms at the electroweak scale. In this Section, we first review flavour violation in the MSSM, present its implementation at the electroweak scale, and elaborate on different non-minimal GMSB models including flavour violation. We then re-analyze the parameter space and show how NMFV can provide a way to relax the stringent constraints challenging the minimal GMSB models.

A. Theoretical Framework

In constrained minimal flavour violation (cMFV) SUSY models, the only source of flavour violation arises through the rotation of the quark interaction eigenstates into the basis of physical mass eigenstates, where the Yukawa matrices are diagonal, as in the SM, and the flavour-violating entries of the squark mass matrices are neglected both at the SUSY-breaking and the weak scale. In SUSY with NMFV, these flavour-violating entries $\Delta_{ij}^{qq'}$ are considered as free parameters. The squared squark mass matrices are then given by

$$M_{\tilde{q}}^2 = \left(\begin{array}{ccc|ccc} M_{L_1}^2 & \Delta_{LL}^{12} & \Delta_{LL}^{13} & m_1 X_1 & \Delta_{LR}^{12} & \Delta_{LR}^{13} \\ \Delta_{LL}^{12*} & M_{L_2}^2 & \Delta_{LL}^{23} & \Delta_{RL}^{12*} & m_2 X_2 & \Delta_{LR}^{23} \\ \Delta_{LL}^{13*} & \Delta_{LL}^{23*} & M_{L_3}^2 & \Delta_{RL}^{13*} & \Delta_{RL}^{23*} & m_3 X_3 \\ \hline m_1 X_1^* & \Delta_{RL}^{12} & \Delta_{RL}^{13} & M_{R_1}^2 & \Delta_{RR}^{12} & \Delta_{RR}^{13} \\ \Delta_{LR}^{12*} & m_2 X_2^* & \Delta_{RL}^{23} & \Delta_{RR}^{12*} & M_{R_2}^2 & \Delta_{RR}^{23} \\ \Delta_{LR}^{13*} & \Delta_{LR}^{23*} & m_3 X_3^* & \Delta_{RR}^{13*} & \Delta_{RR}^{23*} & M_{R_3}^2 \end{array} \right), \quad (6)$$

where $M_{L_k}^2$ and $M_{R_k}^2$ denote their usual diagonal entries,

$$M_{L_k}^2 = M_{Q_k}^2 + m_k^2 + \cos 2\beta \, m_Z^2 (T_k^3 - e_k \sin^2 \theta_W), \quad (7)$$

$$M_{R_k}^2 = M_{U_k, D_k}^2 + m_k^2 + \cos 2\beta \, m_Z^2 e_k \sin^2 \theta_W, \quad (8)$$

and helicity mixing is generated by the elements

$$X_q = A_q^* - \mu \begin{cases} \cot \beta & \text{for up-type squarks,} \\ \tan \beta & \text{for down-type squarks.} \end{cases} \quad (9)$$

Here, θ_W is the electroweak mixing angle, $M_{Q,U,D}$ are the usual SUSY-breaking squark masses, A_q is the trilinear coupling, and m_k , T_k^3 , and e_k denote the mass, weak isospin, and electric charge of the quark q_k , the index k referring to the (s)quark generation. The flavour-violating elements $\Delta_{ij}^{qq'}$ are usually normalized to the diagonal entries [10],

$$\Delta_{ij}^{qq'} = \lambda_{ij}^{qq'} M_{i_q} M_{j_{q'}}, \quad (10)$$

so that NMFV is governed by 24 arbitrary complex dimensionless parameters $\lambda_{ij}^{qq'}$.

The diagonalization of the mass matrices M_u^2 and M_d^2 requires the introduction of two additional 6×6 matrices R^u and R^d , relating the helicity and flavour eigenstates to the physical mass eigenstates through

$$(\tilde{u}_1, \tilde{u}_2, \tilde{u}_3, \tilde{u}_4, \tilde{u}_5, \tilde{u}_6)^T = R^u (\tilde{u}_L, \tilde{c}_L, \tilde{t}_L, \tilde{u}_R, \tilde{c}_R, \tilde{t}_R)^T, \quad (11)$$

$$(\tilde{d}_1, \tilde{d}_2, \tilde{d}_3, \tilde{d}_4, \tilde{d}_5, \tilde{d}_6)^T = R^d (\tilde{d}_L, \tilde{s}_L, \tilde{b}_L, \tilde{d}_R, \tilde{s}_R, \tilde{b}_R)^T. \quad (12)$$

By convention, the squark mass eigenstates are labeled according to $m_{\tilde{q}_1} < \dots < m_{\tilde{q}_6}$ for $q = u, d$. For a detailed review of flavour violation in the MSSM see e.g. Ref. [26]. We stress that we do not employ the mass-insertion approximation with its perturbative expansion in the parameters $\lambda_{ij}^{qq'}$, but rather perform the diagonalization of the squark-mass matrices numerically. Relatively strong constraints on NMFV SUSY models can be obtained from low-energy and electroweak precision observables, e.g. upper limits from the neutral kaon sector, on B - and D -meson oscillations, various rare decays, and electric dipole moments. In several publications [10, 11, 27], rather complete analyses have been presented, pointing out that the down-squark sector is particularly constrained from K - and B -physics processes

with external down-type quarks and that within the mass-insertion approximation the only substantial mixing in the squark sector occurs between the second and third generations in the left-left and right-right chiral sectors. Note that the latter is suppressed in gravity mediation models by the scaling of the corresponding entries $\Delta_{ij}^{qq'}$ with the SUSY breaking scale, while in gauge mediation models the mixing in the left-right chiral sector, induced by A -terms, is small. The up-squark sector is in general less experimentally constrained. This situation may change once additional information from neutral and charged Higgs production and decay becomes available [16, 28]. In our analysis, we apply $SU(2)$ gauge invariance to the left-chiral sector and take implicitly into account the above mentioned constraints by restricting ourselves, also for the sake of simplicity, to the case of two real NMFV parameters,

$$\lambda_{LL} \equiv \lambda_{LL}^{sb} \simeq \lambda_{LL}^{ct} \lesssim 0.2 \quad \text{and} \quad \lambda_{RR} \equiv \lambda_{RR}^{sb} \simeq \lambda_{RR}^{ct} \lesssim 0.2, \quad (13)$$

while all other $\lambda_{ij}^{qq'}$ are zero.

Although the gauge interactions are flavour-blind, it has been shown that there are several possibilities for flavour violation in both the squark and slepton sectors to arise within GMSB models. For example, for very high messenger scales $M_{\text{mes}} \gtrsim 10^{15}$ GeV gravity is no longer negligible with respect to gauge interactions [6]. As a consequence, flavour-violating terms are reintroduced through gravity mediation as in mSUGRA models. However, scenarios with such high messenger scales are rather unattractive from a phenomenological point of view due to the resulting very high SUSY masses. Second, flavour violation can also be induced from heavy right-handed neutrinos participating in leptogenesis [7]. If these are lighter than the messenger scale, flavour off-diagonal mass terms are introduced into the slepton mass matrices. A third possibility might be to consider broken messenger number invariance, that implies that the lightest messenger is not stable and introduces flavour-violating terms in the Lagrangian at the weak scale [6]. A disadvantage of this model is that the now unstable lightest messenger may not be a viable candidate for cold dark matter in the case of a very light gravitino, which cannot account for the observed relic abundance.

For our study, we focus on the model proposed in Ref. [8], based on the introduction of a mixing between messenger and matter fields. In the case of fundamental messenger multiplets belonging to $\mathbf{5}$ and $\bar{\mathbf{5}}$ representations of $SU(5)$, the messengers carry quantum numbers of left-handed leptons and right-handed down-type quarks. As a consequence, flavour violation is introduced into the chiral sectors of right-handed sleptons and left-handed (up- and down-type) squarks. In our analysis of squark flavour violation, this corresponds to including a variation of the parameter λ_{LL} , while λ_{RR} is set to zero. An alternative model with antisymmetric messenger multiplets belonging to $\mathbf{10}$ and $\bar{\mathbf{10}}$ representations can also be considered. In this case, the messengers share quantum numbers with right-handed leptons, left-handed up- and down-type quarks, and right-handed up-type quarks, leading to flavour mixing for left-handed sleptons as well as for both left- and right-handed up- and down-type squarks. Note that, in this antisymmetric scenario, flavour mixing in the sector of right-handed down-type squarks may be parameterized independently of the other squarks. In our analysis, however, we use for simplicity the same flavour violation parameter $\lambda_{LL} = \lambda_{RR}$ for both chiral sectors. We should stress that in both scenarios flavour violation is completely governed by the parameter λ_{LL} .

B. Scans of the Parameter Space and Benchmark Points

We now re-investigate the constraints discussed in Sec. II and include non-minimal flavour violation as discussed above. Allowed regions for the parameters Λ , M_{mes} , N_{mes} , $\tan\beta$, $\text{sgn}(\mu)$, λ_{LL} , and λ_{RR} are obtained by explicitly imposing the constraints from $b \rightarrow s\gamma$, $\Delta\rho$, and a_μ , that are sensitive to flavour-violating terms. In particular, the branching ratio $\text{BR}(b \rightarrow s\gamma)$ is directly affected by the allowed squark mixing between the second and third generation. Squarks enter the calculation at the one-loop level, as do the SM contributions, so that the dependence on the NMFV-parameters is rather important. A second important consequence of NMFV in the MSSM is the generation of a large splitting between squark-mass eigenvalues, which directly influences the electroweak precision variable $\Delta\rho$. Concerning a_μ^{SUSY} , the squark contributions are suppressed with respect to the slepton contributions, so that its dependence on flavour violation is less important. The renormalization group running is again performed with **SPheno** 2.2.3. The flavour violating terms λ_{LL} and λ_{RR} are included in the squark sector at the weak scale as discussed in Sec. III A before diagonalizing the mass matrices and computing the low-energy and electroweak precision observables with **FeynHiggs** 2.6.4.

In Figs. 2 – 7 we show scans of the Λ – M_{mes} plane for $\mu > 0$ and the same values $N_{\text{mes}} = 1, 3$ and $\tan\beta = 15, 30, 50$ as in Sec. II. The region favoured by the anomalous magnetic moment of the muon a_μ (light/grey) is quite insensitive to variations of the parameter λ_{LL} , since dominant SUSY effects come from induced quantum loops of gauginos and sleptons, while squarks contribute only at the two-loop level, which reduces the dependence on squark flavour violation. As expected, the $b \rightarrow s\gamma$ excluded region (dark/blue) depends strongly on flavour mixing, while the constraint coming from $\Delta\rho$ does not play a role for the moderate SUSY masses relevant to our region of interest, so

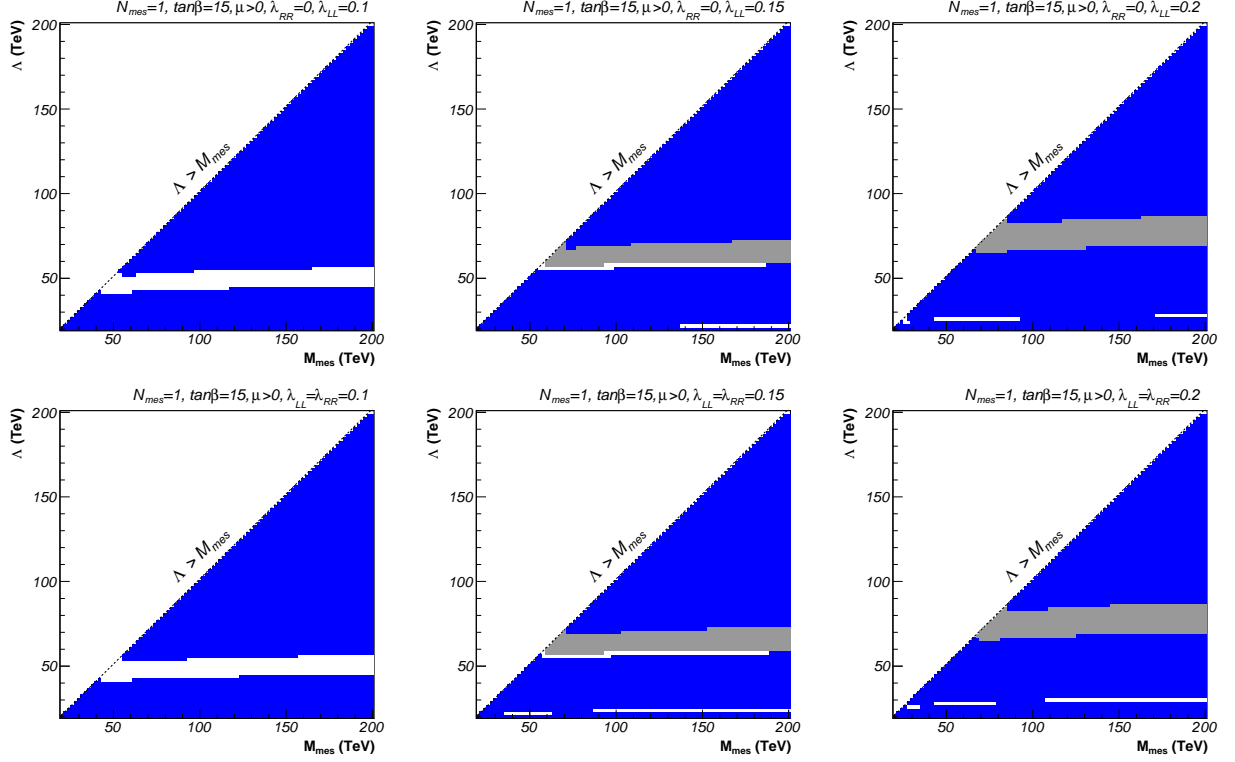


FIG. 2: The Λ - M_{mes} planes for $N_{\text{mes}} = 1$, $\tan \beta = 15$, $\mu > 0$, and $\lambda_{LL} = 0.1, 0.15$ and 0.2 . We show a_μ favoured (light/grey) and $b \rightarrow s\gamma$ excluded (dark/blue) regions of the GMSB parameter space with non-minimal flavour violation in either the left-left chiral ($\lambda_{RR} = 0$, top) or both the left-left and right-right chiral ($\lambda_{RR} = \lambda_{LL}$, bottom) squark sectors. The region where $\Lambda > M_{\text{mes}}$ does not allow for physical solutions of the RGEs.

that the corresponding excluded regions are not shown. Note that the difference between the two flavour violation scenarios considered here is relatively small, as can be seen in Figs. 2 – 7. It becomes clear that, if we allow for flavour mixing between the second and third generation squarks, windows in the parameter space both favoured by a_μ and not excluded by the stringent constraint from $b \rightarrow s\gamma$ make their appearance for small and moderate SUSY masses.

Within these regions, we propose six benchmark scenarios permitting non-minimal flavour violation and not yielding too high SUSY masses (“collider-friendly”), so that possible SUSY signals should be observable at present and/or future hadron colliders. Our choices are presented in Tab. I, labeled starting at the point E due to our four benchmark proposals for mSUGRA scenarios including NMFV [12]. Note that, in contrast to the mSUGRA case, these scenarios are not valid assuming cMFV ($\lambda_{LL} = \lambda_{RR} = 0$), so that we indicate the allowed ranges for our flavour mixing parameter λ_{LL} .

Starting with $\tan \beta = 15$ and $N_{\text{mes}} = 1$ (see Fig. 2), we choose our benchmark point E in the region both favoured by the electroweak precision constraints and corresponding to rather light SUSY particles. As for any GMSB scenario, the gravitino is the lightest SUSY particle (LSP). The next-to-lightest SUSY particle (NLSP) is the lightest neutralino with $m_{\tilde{\chi}_1^0} = 95.4$ GeV, but the three lightest charged sleptons are very close with similar masses around 100 GeV. The other sleptons, sneutrinos, and gauginos have moderate masses of about 150 – 300 GeV, while the squarks and gluino are quite heavy with masses lying in the range of 700 – 800 GeV. However, they are much lighter than those corresponding to the point SPS 8 with its larger values of Λ and M_{mes} , lie well above the experimental limits obtained from direct searches assuming cMFV, and are experimentally accessible at the LHC.

The point F (see Fig. 3) differs very little from the point SPS 7, with the SUSY-breaking scale Λ shifted from 40 to 30 TeV, so that it now lies in the preferred region with respect to the $b \rightarrow s\gamma$ constraint. As for SPS 7, the three lightest sleptons have masses around 100 GeV, the lightest being the stau with $m_{\tilde{\tau}_1} = 90.7$ GeV. The other sleptons, sneutrinos, and gauginos are a bit heavier (120-200 GeV), and the squarks and gluino are rather heavy (600-700 GeV).

The points G, H, I, and J (see Figs. 4-7) all have a stau NLSP with a mass between 99 and 160 GeV. The main difference in their spectra is the number and nature of the particles that are closest in mass to the NLSP. For the point G, these are two sleptons and the lightest neutralino, whereas for the point H these are only the two sleptons.

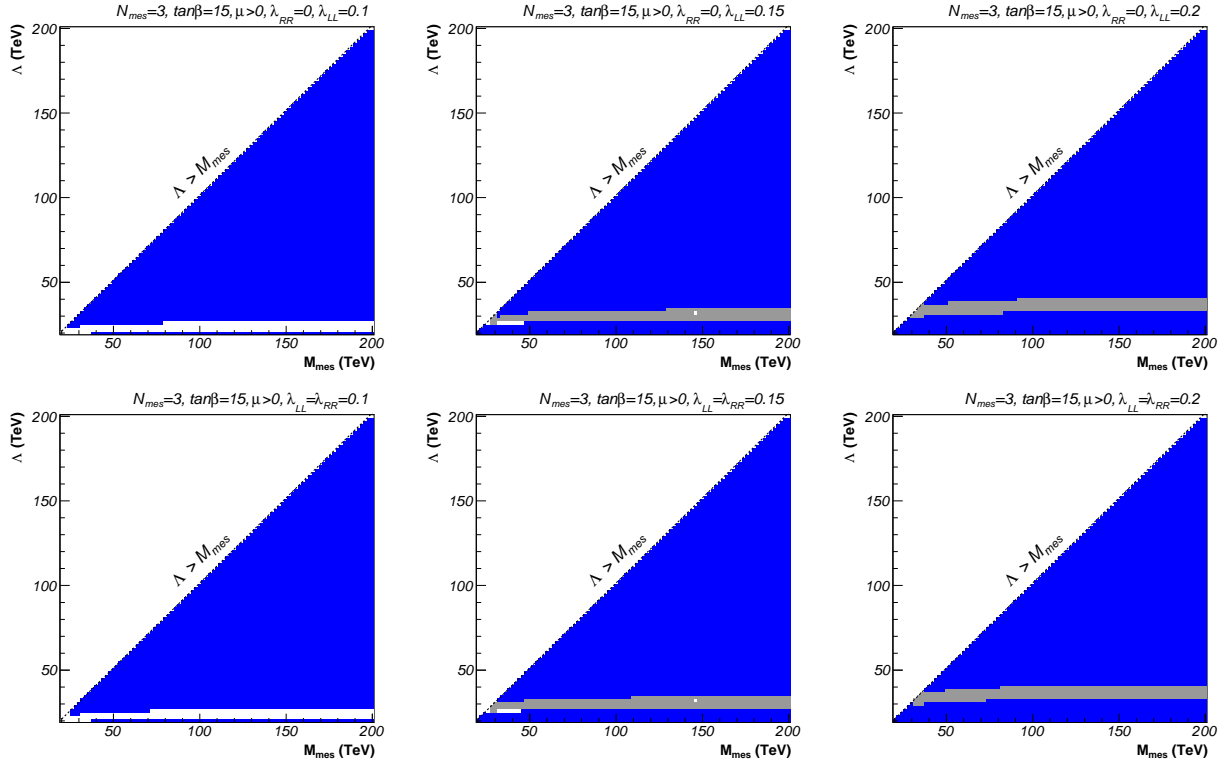


FIG. 3: Same as Fig. 2 for $N_{\text{mes}} = 3$ and $\tan \beta = 15$.

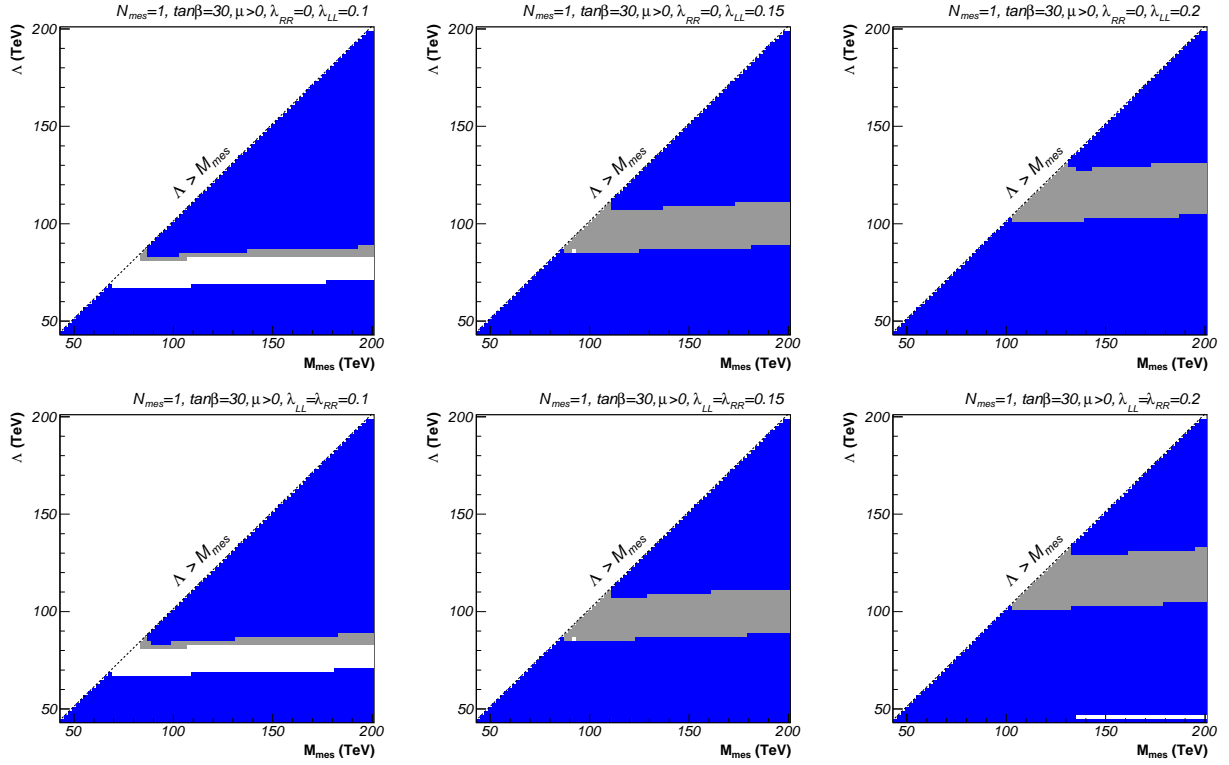
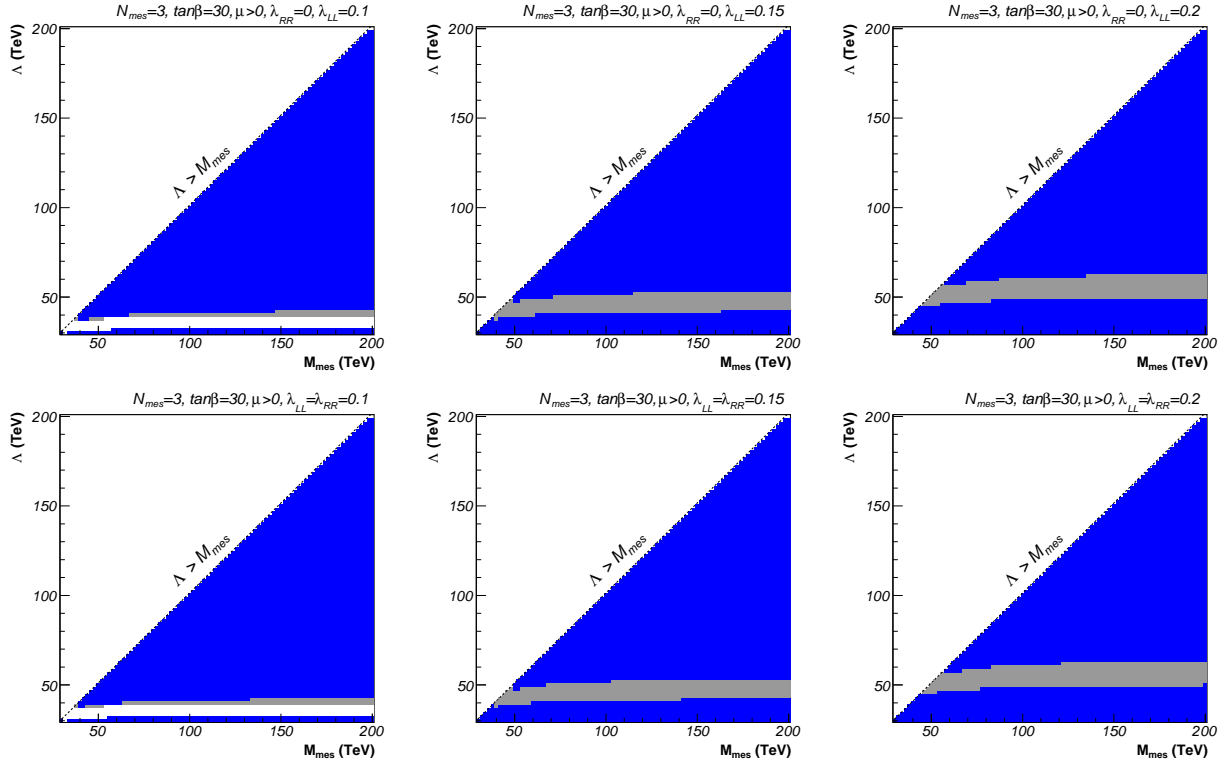
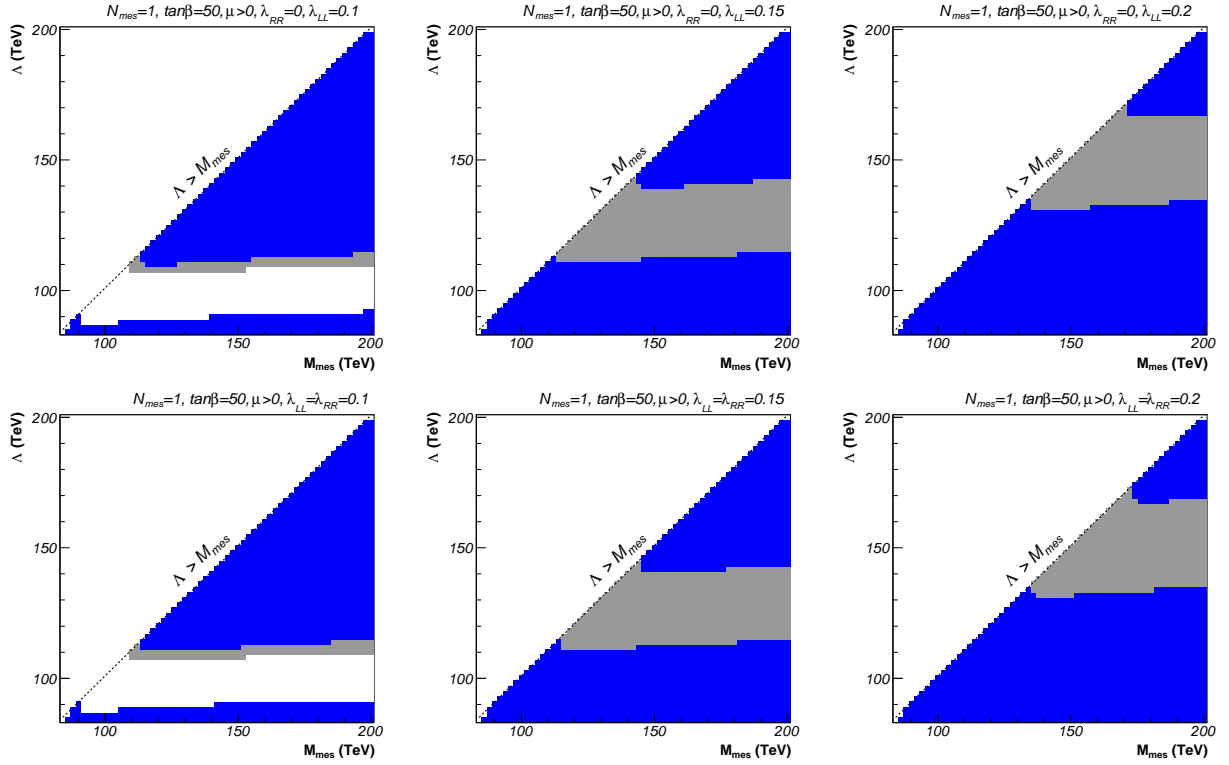


FIG. 4: Same as Fig. 2 for $N_{\text{mes}} = 1$ and $\tan \beta = 30$.

FIG. 5: Same as Fig. 2 for $N_{\text{mes}} = 3$ and $\tan \beta = 30$.FIG. 6: Same as Fig. 2 for $N_{\text{mes}} = 1$ and $\tan \beta = 50$.

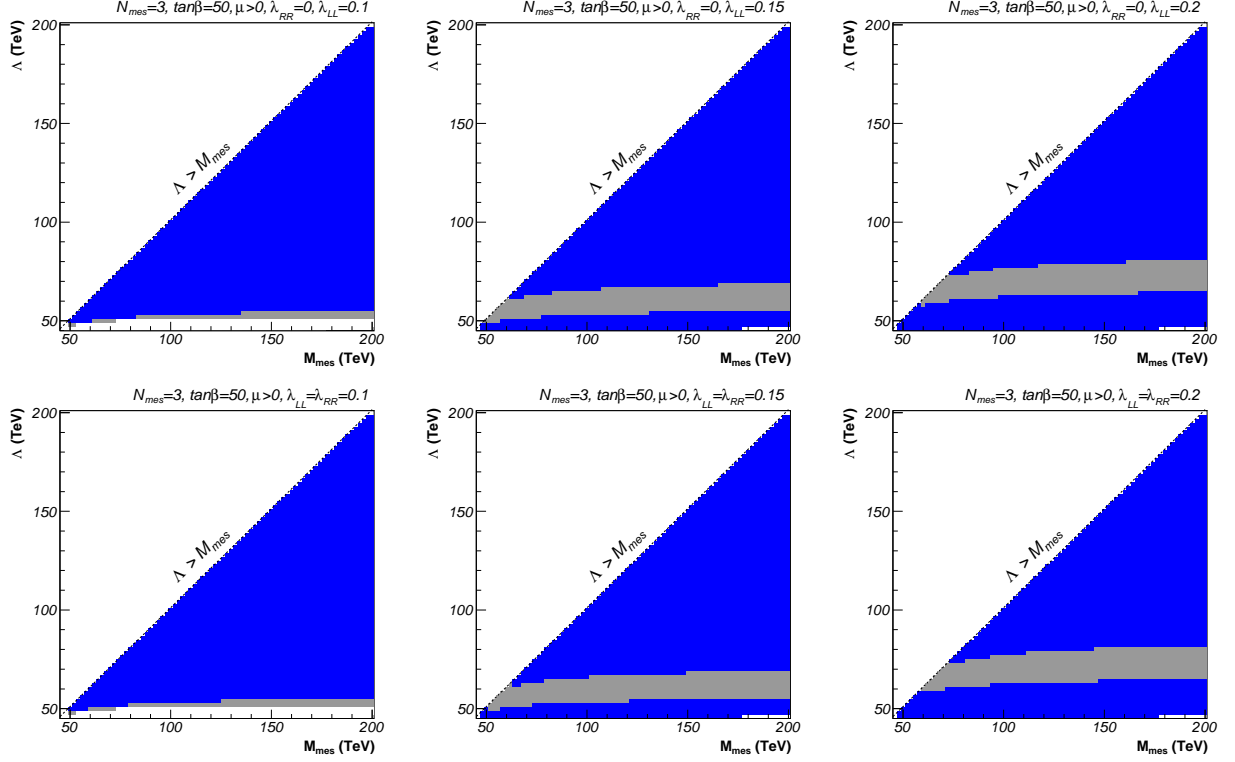


FIG. 7: Same as Fig. 2 for $N_{\text{mes}} = 3$ and $\tan \beta = 50$.

TABLE I: GMSB benchmark points allowing for non-minimal flavour violation in the left-left ($\lambda_{RR} = 0$) or both the left-left and right-right ($\lambda_{RR} = \lambda_{LL}$) chiral squark sectors. We also indicate the allowed range for the NMFV-parameter λ_{LL} , the nature of the next-to-lightest SUSY particle (NLSP), and the closest SPS benchmark point (if relevant), which are valid for both flavour-violating scenarios.

	Λ [TeV]	M_{mes} [TeV]	N_{mes}	$\tan \beta$	$\text{sgn}(\mu)$	λ_{LL}	NLSP	SPS
E	65	90	1	15	+	[0.14, 0.20]	$\tilde{\chi}_1^0$	8
F	30	80	3	15	+	[0.12, 0.18]	$\tilde{\tau}_1$	7
G	100	110	1	30	+	[0.14, 0.20]	$\tilde{\tau}_1$	—
H	45	100	3	30	+	[0.12, 0.18]	$\tilde{\tau}_1$	—
I	130	140	1	50	+	[0.14, 0.20]	$\tilde{\tau}_1$	—
J	60	100	3	50	+	[0.14, 0.20]	$\tilde{\tau}_1$	—

The points I and J do not have any particles close to the NLSP in mass. For the four points G, H, I, and J, the other sleptons and gauginos are rather light (200-600 GeV), while the squarks and the gluino are very heavy (1-1.5 TeV).

We now study in detail the dependence of the electroweak precision and low-energy observables as well as the mass spectra of the points E, F, G, H, I, and J. In Figs. 8 – 13, we show the corresponding branching ratio $\text{BR}(b \rightarrow s\gamma)$ (top left) and the observable $\Delta\rho$ (bottom left) as a function of the NMFV-parameter λ_{LL} . We include both flavour violation scenarios, the one for fundamental messengers with $\lambda_{RR} = 0$ as well as the one with antisymmetric messengers, where $\lambda_{RR} = \lambda_{LL}$. As already mentioned, the leptonic observable a_μ depends only very weakly (at the two-loop level only) on the squarks. As a consequence, we find values of a_μ independent of λ_{LL} for our six benchmark scenarios, which are $a_\mu^{\text{SUSY}} = 37.7 \cdot 10^{-10}$, $41.3 \cdot 10^{-10}$, $31.4 \cdot 10^{-10}$, $36.6 \cdot 10^{-10}$, $31.8 \cdot 10^{-10}$, and $34.2 \cdot 10^{-10}$ for the points E, F, G, H, I, and J, respectively. These values lie well within 2σ of the experimentally favoured range of Eq. (4), and even within 1σ for the points E, G, H, I, and J. For the inclusive branching ratio $\text{BR}(b \rightarrow s\gamma)$, the experimentally allowed range within 2σ is indicated by two horizontal dashed lines. The good agreement between the measurements and

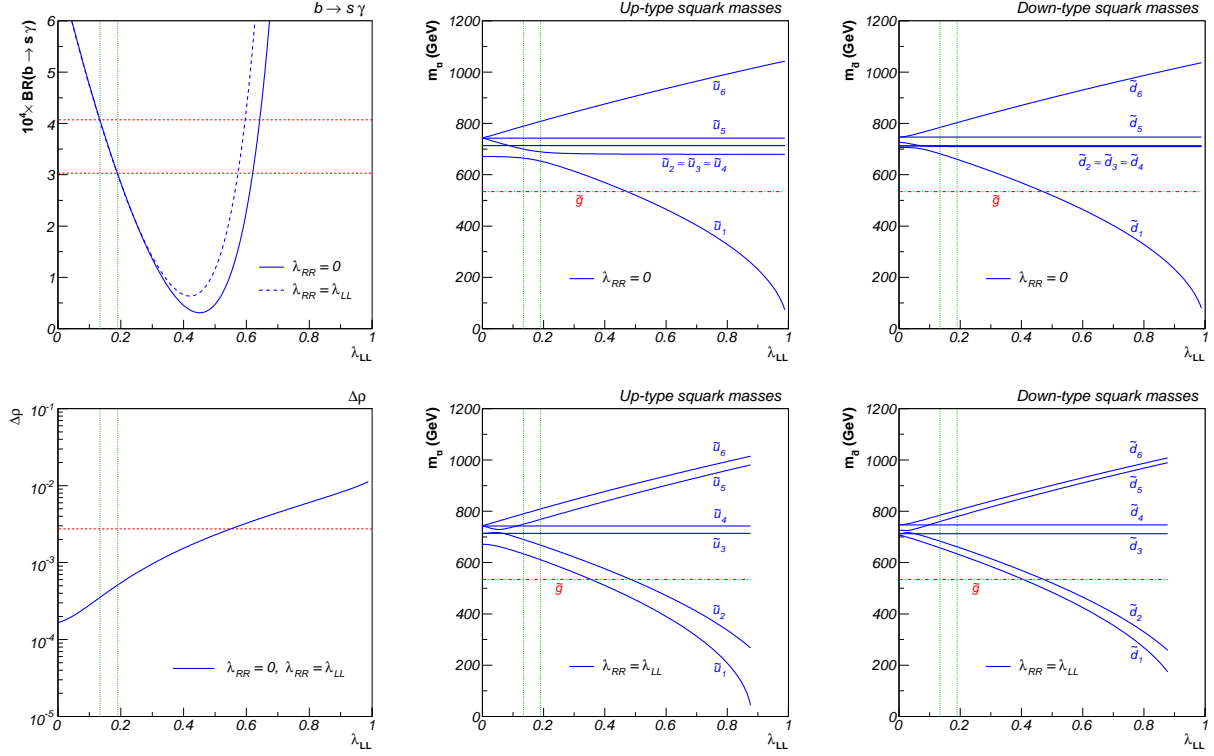


FIG. 8: Dependence of the precision variables $\text{BR}(b \rightarrow s\gamma)$ and $\Delta\rho$ as well as of the up- and down-type squark masses on the NMFV-parameter λ_{LL} for flavour mixing in the left-left ($\lambda_{RR} = 0$) or both the left-left and right-right ($\lambda_{RR} = \lambda_{LL}$) chiral squark sectors for our benchmark scenario E. The experimentally allowed ranges within 2σ are indicated by horizontal dashed lines. The vertical dotted lines indicate the allowed range for λ_{LL} with respect to the most stringent constraint from $b \rightarrow s\gamma$. For $\lambda_{LL} = \lambda_{RR} \geq 0.9$ no physical solutions are possible.

the two-loop SM prediction in combination with the strong dependence of the SUSY contribution on squark flavour mixing only leave two allowed narrow intervals for our flavour violation parameter, one being at relatively low values of $\lambda_{LL} \sim 0.15$, the second one at higher values of $\lambda_{LL} \sim 0.5 - 0.7$. It is well known that the latter is disfavoured by $b \rightarrow s\mu^+\mu^-$ data [29]. The remaining one is indicated by vertical dotted lines. Note that the difference between the two scenarios is small for the relevant values of $\lambda_{LL} \lesssim 0.2$. Concerning the observable $\Delta\rho$, the difference between the two considered flavour mixing scenarios is not visible, so that only one curve is shown. Again, the horizontal line indicates the favoured range within 2σ , where only the upper limit is visible on our logarithmic scale. In contrast to $\text{BR}(b \rightarrow s\gamma)$, here the relatively large experimental errors allow for values of $\lambda_{LL} \lesssim 0.3 - 0.6$, depending on the benchmark point. The vertical dashed lines indicate the allowed range for λ_{LL} with respect to the more stringent constraint coming from $b \rightarrow s\gamma$.

The difference between the two flavour violation scenarios becomes more obvious when we study the squark mass eigenvalues. The up- and down-type squark masses are shown as a function of the flavour mixing parameter λ_{LL} in the centre and right upper panels of Figs. 8 – 13 for mixing with fundamental messengers ($\lambda_{RR} = 0$) and in the centre and right lower panels for antisymmetric messengers ($\lambda_{RR} = \lambda_{LL}$). We observe here the same level-reordering phenomenon between neighbouring states as already in the case of minimal supergravity, discussed in Ref. [12]. With increasing flavour violation the mass splitting between the lightest and heaviest mass eigenstates becomes larger, while the intermediate squark masses are practically unchanged. At the points, where two levels should cross, we observe so-called “avoided crossings” of the mass eigenvalues. This phenomenon of level-reordering is due to the fact that the mass matrices depend on a single real parameter λ_{LL} . Unfortunately, many “avoided crossings” lie below, but some also within the allowed ranges of the flavour-violating parameter λ_{LL} , indicated by green vertical lines for each of the six benchmark scenarios. The level-reordering phenomenon is of similar importance for up-type and down-type squarks. Concerning the difference between our two implementations of flavour violation in the squark matrices, we observe an important splitting for only the lightest and heaviest eigenstates in the case of flavour mixing only in the left-left chiral sector. In contrast, for flavour violation in both the left-left and right-right chiral squark sectors,

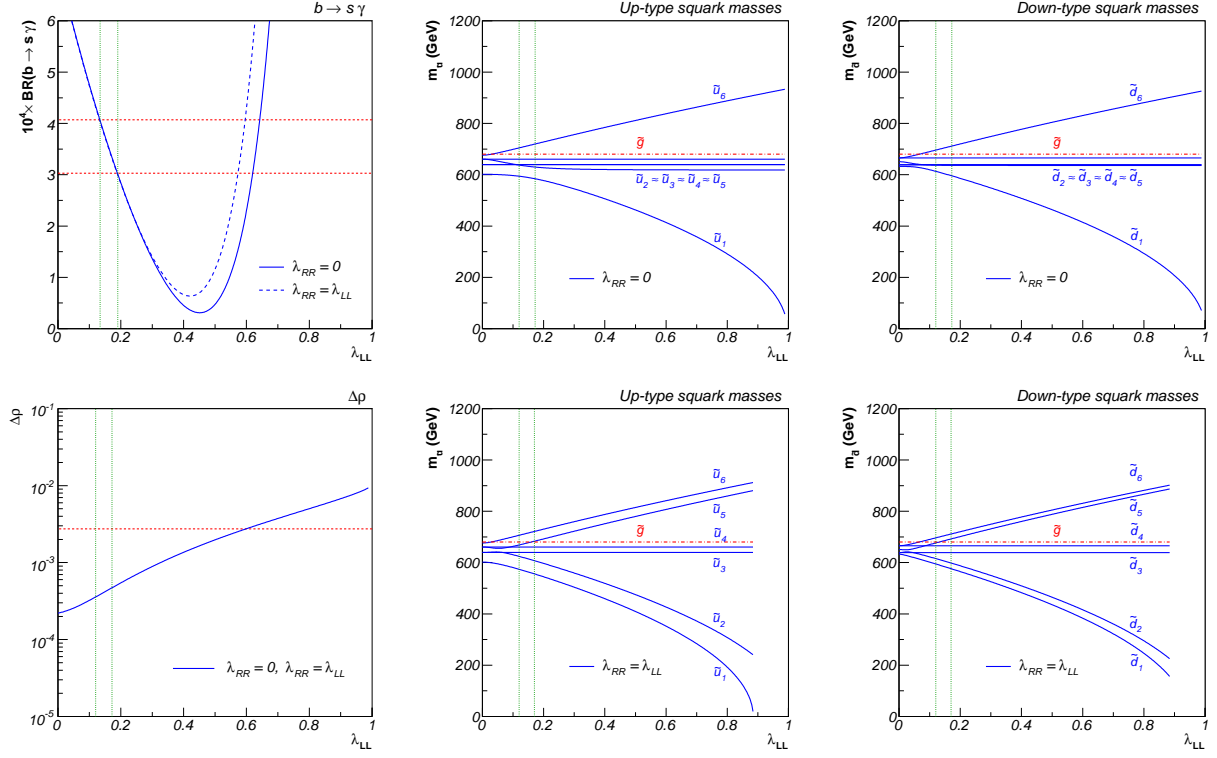


FIG. 9: Same as Fig. 8 for our benchmark scenario F.

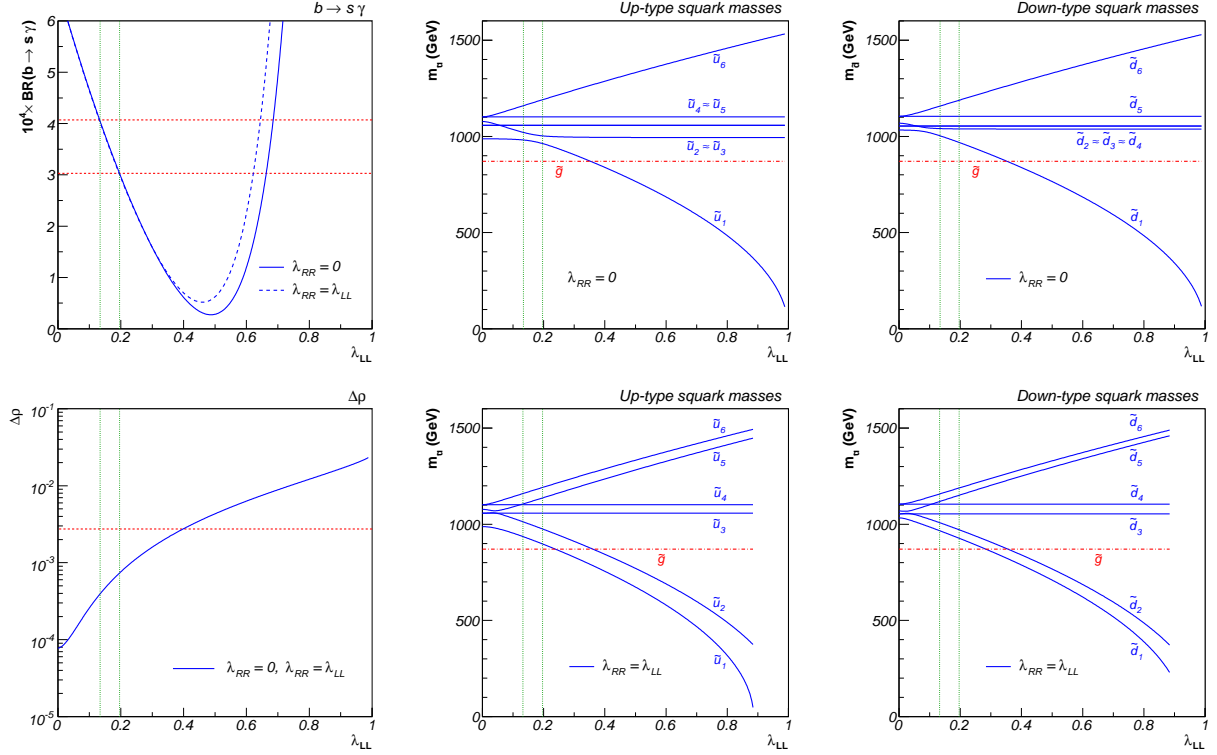


FIG. 10: Same as Fig. 8 for our benchmark scenario G.

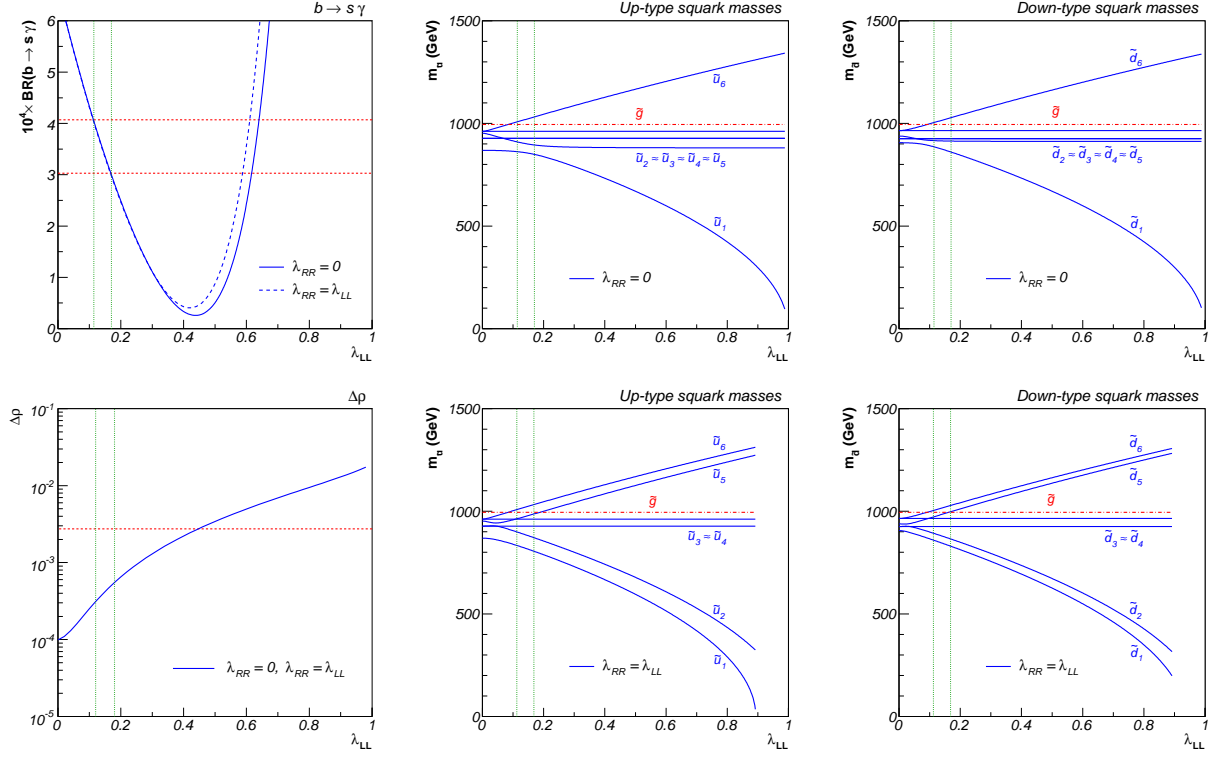


FIG. 11: Same as Fig. 8 for our benchmark scenario H.

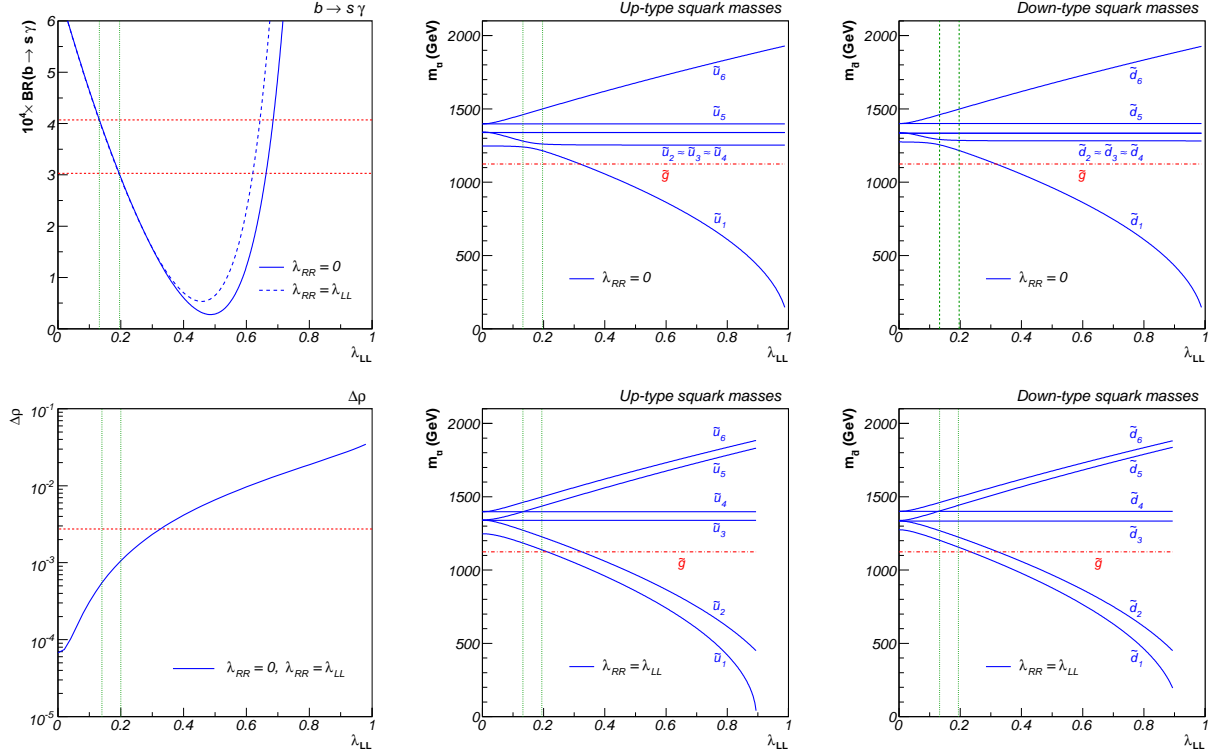


FIG. 12: Same as Fig. 8 for our benchmark scenario I.

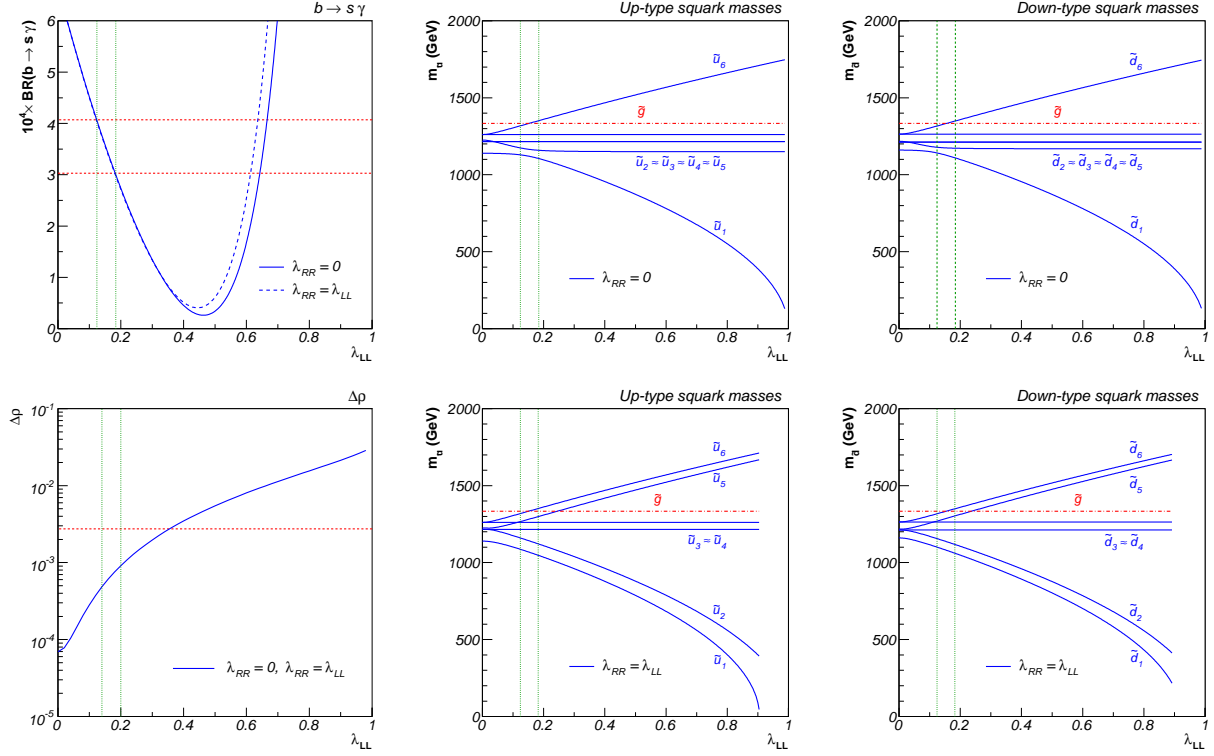


FIG. 13: Same as Fig. 8 for our benchmark scenario J.

the two lightest and two heaviest mass eigenvalues give rise to an important splitting, while only the remaining two masses are practically independent of λ_{LL} . This is a direct consequence of the fact that we have introduced additional flavour mixing in two distinct sectors of the squark mass matrices, and this will influence the squark and gaugino production cross sections presented in Sec. V. Note also that in the case of flavour mixing only in the left-left chiral sector, “avoided” level crossings occur among the $\tilde{q}_{1,2}$, $\tilde{q}_{3,4}$, and $\tilde{q}_{5,6}$ mass eigenstates, whereas in the case of flavour mixing in both the left-left and right-right chiral squark sectors, we rather observe the mass flips among the $\tilde{q}_{2,3}$ and $\tilde{q}_{4,5}$ mass eigenstates, respectively.

IV. COSMOLOGICAL CONSTRAINTS

To be cosmologically viable, a supersymmetric model should include a convincing candidate for the cold dark matter (CDM) in our Universe. This particle has to be stable, electrically neutral, and a colour singlet [30, 31]. Furthermore its relic density has to lie within the range

$$0.094 \leq \Omega_{\text{CDM}} h^2 \leq 0.136 \quad (14)$$

at 95% (2σ) confidence level. Here, h denotes the present Hubble expansion rate in units of $100 \text{ km s}^{-1} \text{ Mpc}^{-1}$. This limit has been obtained from the three-year data of the WMAP satellite, combined with recent SDSS and SNLS survey and Baryon Acoustic Oscillation data, and interpreted within an eleven-parameter inflationary model [32], which is more general than the usual six-parameter “vanilla” concordance model of cosmology. Note that this range is well compatible with the older, independently obtained range of $0.094 \leq \Omega_{\text{CDM}} h^2 \leq 0.129$ of Ref. [33].

A natural candidate in SUSY models is the lightest supersymmetric particle (LSP), which is the gravitino in GMSB models. Depending on its mass, the gravitino can account either for cold ($m_{\tilde{G}} \gtrsim 100 \text{ keV}$), for warm ($1 \text{ keV} \lesssim m_{\tilde{G}} \lesssim 100 \text{ keV}$), or for hot ($m_{\tilde{G}} \lesssim 1 \text{ keV}$) dark matter. Today’s gravitino abundance in the Universe has two contributions. First, gravitinos are produced by thermal scattering in the very early Universe. The corresponding energy density

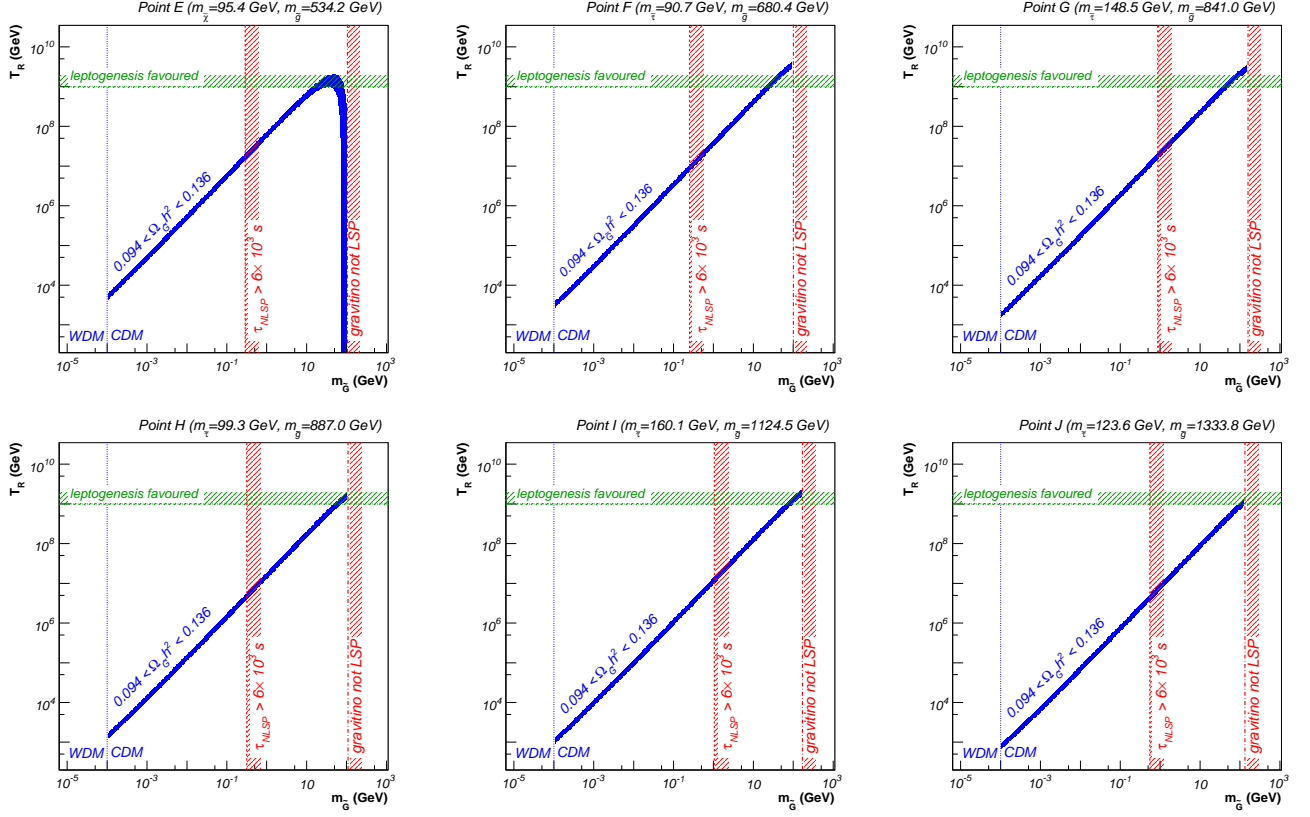


FIG. 14: The cosmologically favoured regions in the $m_{\tilde{G}}-T_R$ plane for our benchmark scenarios E, F, G, H, I, and J with respect to WMAP data (dark/blue), the NLSP lifetime (vertical red line), and leptogenesis (horizontal green line). Also indicated are the limits between gravitino warm (WDM) or cold (CDM) dark matter and the regions where the gravitino would not be the LSP.

[34–36]

$$\Omega_{\tilde{G}}^{\text{th}} h^2 \simeq 0.27 \left(\frac{T_R}{10^{10} \text{ GeV}} \right) \left(\frac{100 \text{ GeV}}{m_{\tilde{G}}} \right) \left(\frac{m_{\tilde{g}}}{1 \text{ TeV}} \right)^2 \quad (15)$$

involves the gluino mass $m_{\tilde{g}}$ at low energy and the reheating temperature T_R . The latter is the temperature of the Universe after inflation, for which at present no stringent constraints exist. Values of $T_R \gtrsim 10^9$ GeV are preferred in scenarios that feature leptogenesis in order to explain the cosmic baryon asymmetry [37]. As the resummation method leading to Eq. (15) may become unreliable below $T_R \simeq 10^7$ GeV, we use the more accurate result given in [38] and do not make practical use of the low-temperature region (see below). Note that the thermal gravitino relic density may also be affected by late-time entropy production coming, e.g., from the decay of the messengers.

Second, there is non-thermal production through decay of the next-to-lightest supersymmetric particle (NLSP) into the gravitino. As each NLSP will decay into its Standard Model partner and one gravitino, the resulting gravitino energy density can be obtained through

$$\Omega_{\tilde{G}}^{\text{non-th}} h^2 = \frac{m_{\tilde{G}}}{m_{\text{NLSP}}} \Omega_{\text{NLSP}}^{\text{th}} h^2, \quad (16)$$

where $\Omega_{\text{NLSP}}^{\text{th}} h^2$ is the thermal freeze-out relic density the NLSP would have if it did not decay. Note that for low values of $m_{\tilde{G}}$ and/or high reheating temperatures T_R thermal production dominates, whereas for high values of $m_{\tilde{G}}$ it is negligible with respect to the contribution from NLSP decay. The NLSP would-be relic density $\Omega_{\text{NLSP}}^{\text{th}} h^2$ is calculated by solving the Boltzmann equation and can be evaluated numerically for any type of NLSP using the public code `micrOMEGAs` [39], whereas the programme `DarkSUSY` [40] is only adapted to the neutralino case. We therefore always use `micrOMEGAs` in this work.

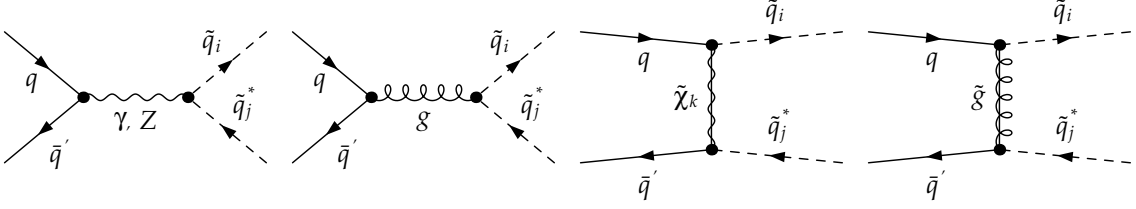


FIG. 15: Tree-level Feynman diagrams for the production of neutral squark-antisquark pairs in quark-antiquark collisions.

Another constraint for scenarios with gravitino dark matter arises from the fact that the NLSP spoils the abundances of light elements in our Universe, if it does not decay rapidly enough [35]. The lifetime of a supersymmetric particle decaying into its Standard Model partner and a gravitino is given by the inverse of the corresponding decay rate. Neglecting here flavour violation and any SUSY particle mixing, which have only little impact [12], we obtain for the lifetime of the NLSP

$$\tau_{\text{NLSP}} \simeq (6.1 \cdot 10^3 \text{s}) \left(\frac{1 \text{ TeV}}{m_{\text{NLSP}}} \right)^5 \left(\frac{m_{\tilde{G}}}{100 \text{ GeV}} \right)^2, \quad (17)$$

where we have inserted the value of the reduced Planck mass $M_{\text{P}} = (8\pi G_{\text{N}})^{-1/2}$ and $G_{\text{N}} = 6.7097 \cdot 10^{-39} \text{ GeV}^{-2}$ [13]. In order to preserve the abundances of the light elements, that are well explained by primordial nucleosynthesis, the lifetime of the NLSP should be shorter than $\tau_{\text{NLSP}} \lesssim 6 \cdot 10^3$ seconds [41]. As a consequence, the latter constraint favours scenarios having a light gravitino, which might enter in conflict with the thermal production favouring a rather high reheating temperature and therefore a rather high gravitino mass, as can be seen from Eq. (15).

In the case of gravitino cold dark matter, we compute the gravitino energy density $\Omega_{\tilde{G}} h^2$ in our Universe as described above, taking into account the contributions from thermal production in the early Universe and from NLSP decay. In Fig. 14, we compare the obtained gravitino relic density to the 2σ range of the cold dark matter relic density of Eq. (14) as a function of the gravitino mass $m_{\tilde{G}}$ and the reheating temperature T_{R} for our benchmark scenarios E to J. For each of the six scenarios, we also indicate the upper limit on the gravitino mass coming from the constraint on the NLSP lifetime, the limit between warm (WDM) and cold dark matter (CDM), as well as the region where the gravitino would become heavier than the NLSP. Concerning the reheating temperature, we indicate the favoured region with respect to leptogenesis above $T_{\text{R}} \sim 10^9 \text{ GeV}$.

Note that the contribution to $\Omega_{\tilde{G}} h^2$ from NLSP decay is only relevant for our point E with its neutralino NLSP and a rather important neutralino energy density $\Omega_{\text{NLSP}}^{\text{th}} h^2 = 0.1275$. The fact that this value lies already within the interval favoured by WMAP opens an allowed band around $m_{\tilde{G}} \approx m_{\tilde{\chi}_1^0} = 95.4 \text{ GeV}$, as can be seen in the first panel of Fig. 14. For the other points, the annihilation cross section of the charged stau NLSP is more important, so that the resulting relic NLSP density is quite low ($\Omega_{\text{NLSP}}^{\text{th}} h^2 \sim 0.003 - 0.012$) and its values lie below the lower limit 0.094 of the WMAP 2σ range.

From the graphs in Fig. 14 it becomes clear that for the chosen “collider-friendly” benchmark points, we cannot fulfill all three cosmological constraints at the same time. For instance, if we want a scenario featuring leptogenesis, i.e. having $T_{\text{R}} > 10^9 \text{ GeV}$, the lifetime of the next-to-lightest SUSY particle (NLSP) would be too long for not spoiling the light element abundances. We therefore relax the less stringent constraint, which is the one coming from leptogenesis.

If we then impose the constraint due to the lifetime of the NLSP, our six benchmark scenarios all lead to an upper limit on the gravitino mass of the order of $m_{\tilde{G}} \lesssim 10^{-1} - 1 \text{ GeV}$. For simplicity, we propose the same value $m_{\tilde{G}} = 10^{-1} \text{ GeV}$ for all points. This respects the limit due to the NLSP lifetime, allows for gravitino cold dark matter with relic gravitino density that agrees with current WMAP data, and this in combination with relatively high values of $T_{\text{R}} \sim 10^7 \text{ GeV}$ for the reheating temperature.

V. SUPERSYMMETRIC PARTICLE PRODUCTION AT THE LHC

In this Section, we present numerical predictions for the production cross sections of squark-antisquark pairs, squark pairs, the associated production of squarks and gauginos, and gaugino pairs in NMFV SUSY at the LHC, i.e. for pp -collisions at $\sqrt{S} = 14 \text{ TeV}$ centre-of-momentum energy. Total unpolarized hadronic cross sections

$$\sigma = \int_{4m^2/S}^1 d\tau \int_{-1/2 \ln \tau}^{1/2 \ln \tau} dy \int_{t_{\min}}^{t_{\max}} dt f_{a/A}(x_a, M_a^2) f_{b/B}(x_b, M_b^2) \frac{d\hat{\sigma}}{dt} \quad (18)$$

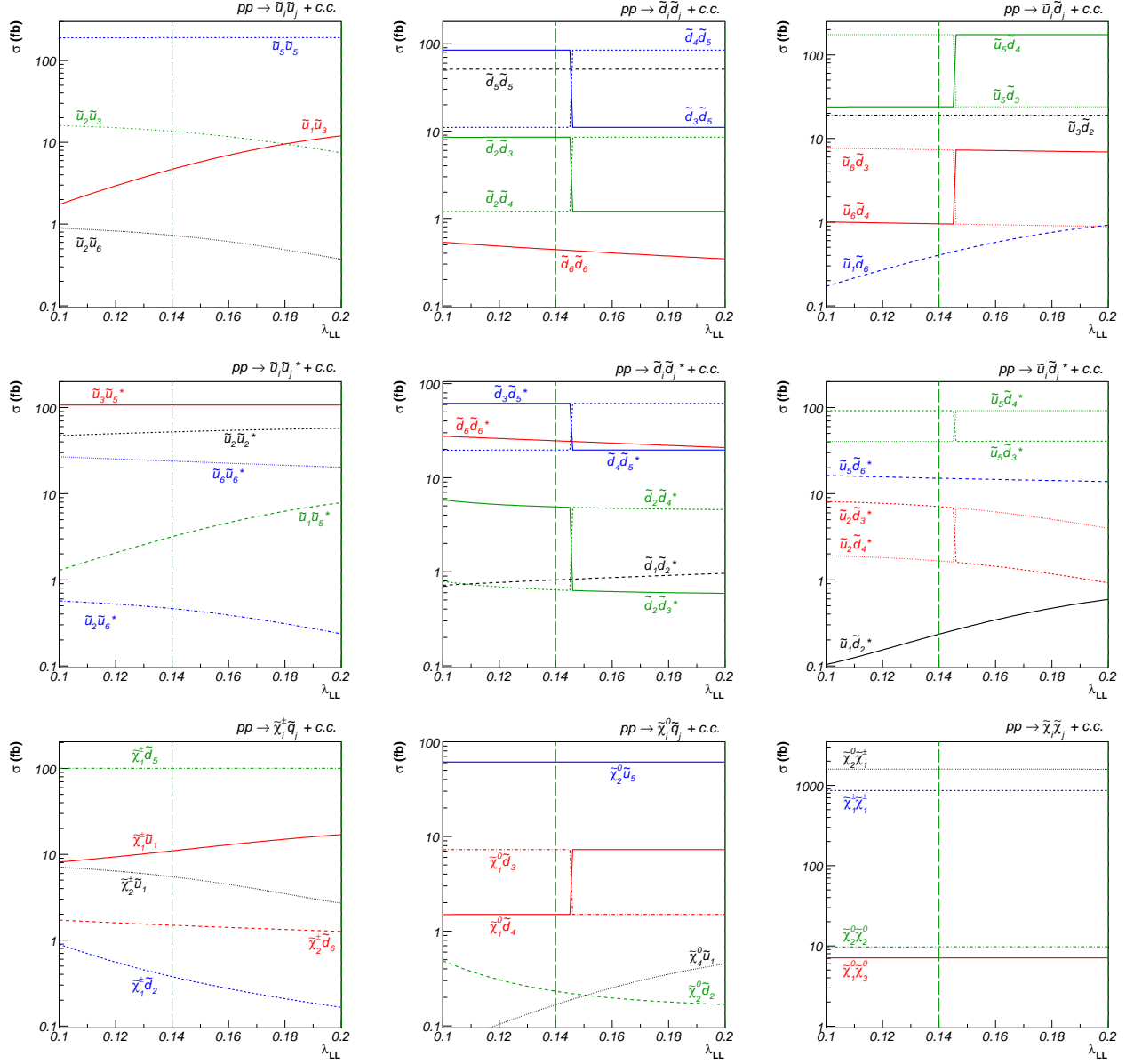


FIG. 16: Examples of cross sections for charged squark-squark pair production, neutral and charged squark-antisquark pair production, associated production of squarks with charginos and neutralinos, and gaugino-pair production at the LHC in our benchmark scenario E with flavour violation in the left-left chiral sector ($\lambda_{RR} = 0$).

are obtained through convolving the relevant partonic cross sections $d\hat{\sigma}/dt$ with universal parton densities $f_{a/A}$ and $f_{b/B}$ of partons a, b in the hadrons A, B , which depend on the longitudinal momentum fractions of the two partons $x_{a,b} = \sqrt{\tau} e^{\pm y}$ and on the unphysical factorization scales $M_{a,b}$. For consistency with our leading order (LO) QCD calculation in the collinear approximation, where all quark masses but the top mass are neglected with respect to the centre-of-momentum energy \sqrt{S} , we employ the LO set of the latest CTEQ6 global parton density fit [42], which includes $n_f = 5$ “light” quark flavours and the gluon, but no top-quark density. Whenever it occurs, i.e. for gluon initial states and gluon or gluino exchanges, the strong coupling constant $\alpha_s(\mu_R)$ is calculated with the corresponding LO value of $\Lambda_{\text{LO}}^{n_f=5} = 165$ MeV. We identify the renormalization scale μ_R with the factorization scales $M_a = M_b$ and set the scales to the average mass of the produced SUSY particles m .

Analytic expressions for the relevant partonic cross sections can be found in Ref. [12]. In particular, neutral squark-antisquark pair production can proceed from a neutral quark-antiquark pair in the initial state. At the tree-level, there are electroweak (s -channel photon- or Z - and t -channel neutralino- or chargino-exchange) and strong (s -channel gluon- and t -channel gluino-exchange) contributions. The contributing Feynman diagrams are shown in Fig. 15,

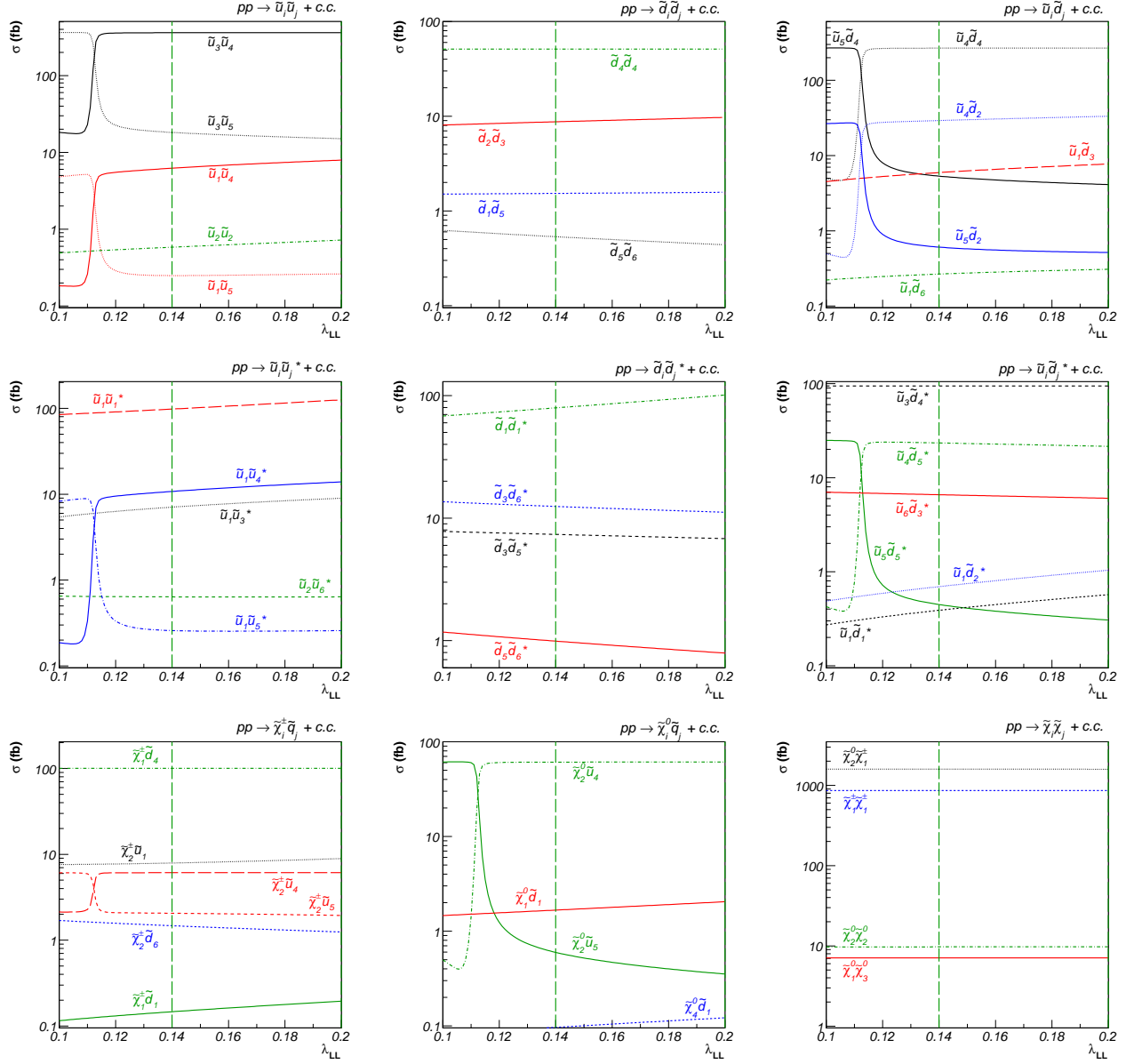


FIG. 17: Same as Fig. 16 for our benchmark scenario E with flavour violation in the left-left and right-right chiral sectors ($\lambda_{RR} = \lambda_{LL}$).

where the chargino contribution in the third diagram is missing in the expressions given in Ref. [12]. The chargino exchanges, which are numerically unimportant for the dominating channels, have to be taken into account for up-type (down-type) quarks in the initial state and down-type (up-type) squarks in the final state. The corrected expression for the quark-initiated differential partonic cross section (Eq. (28) in Ref. [12]) reads

$$\begin{aligned}
 \frac{d\hat{\sigma}_{h_a, h_b}^{q\bar{q}'}}{dt} = & \left(1 - h_a\right)\left(1 + h_b\right) \left[\frac{\mathcal{Y}}{s^2} + \frac{\mathcal{Z}_1}{s_z^2} + \frac{\mathcal{G}}{s^2} + \frac{\tilde{\mathcal{G}}_{11}}{t_{\tilde{g}}^2} + \frac{[\mathcal{Y}\mathcal{Z}]_1}{s s_z} + \frac{[\tilde{\mathcal{G}}\mathcal{Y}]_1}{t_{\tilde{g}} s} + \frac{[\tilde{\mathcal{G}}\mathcal{Z}]_1}{t_{\tilde{g}} s_z} + \frac{[\tilde{\mathcal{G}}\mathcal{G}]_1}{t_{\tilde{g}} s} + \sum_{k,l=1,\dots,4} \left(\frac{\mathcal{N}_{11}^{kl}}{t_{\tilde{\chi}_k^0} t_{\tilde{\chi}_l^0}} \right) \right. \\
 & \left. + \sum_{k=1,\dots,4} \left(\frac{[\mathcal{N}\mathcal{Y}]_1^k}{t_{\tilde{\chi}_k^0} s} + \frac{[\mathcal{N}\mathcal{Z}]_1^k}{t_{\tilde{\chi}_k^0} s_z} + \frac{[\mathcal{N}\mathcal{G}]_1^k}{t_{\tilde{\chi}_k^0} s} \right) + \sum_{k,l=1,2} \left(\frac{c_{11}^{kl}}{t_{\tilde{\chi}_k^\pm} t_{\tilde{\chi}_l^\pm}} \right) + \sum_{k=1,2} \left(\frac{[\mathcal{C}\mathcal{Y}]_1^k}{t_{\tilde{\chi}_k^\pm} s} + \frac{[\mathcal{C}\mathcal{Z}]_1^k}{t_{\tilde{\chi}_k^\pm} s_z} + \frac{[\mathcal{C}\mathcal{G}]_1^k}{t_{\tilde{\chi}_k^\pm} s} \right) \right]
 \end{aligned}$$

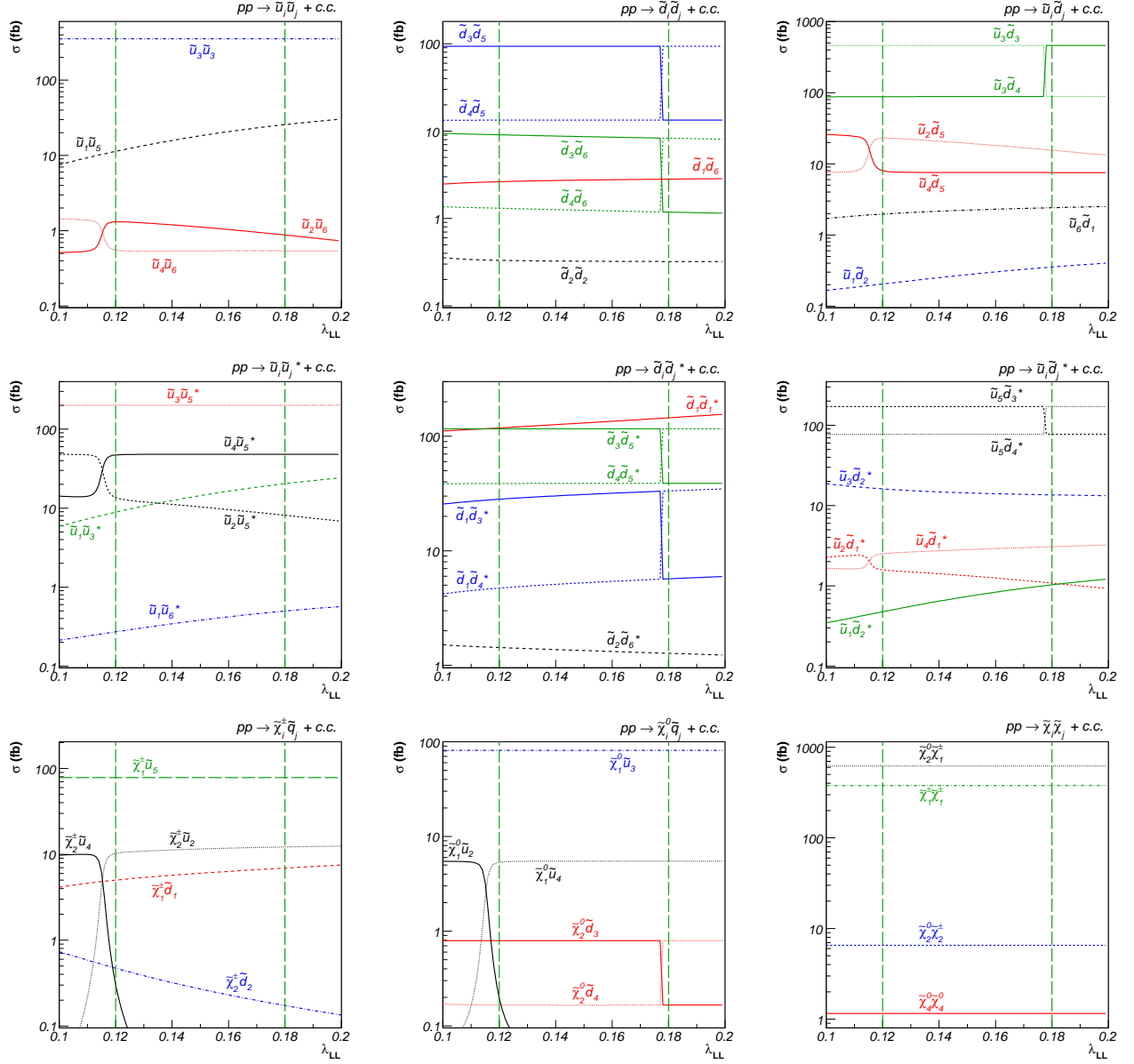


FIG. 18: Same as Fig. 16 for our benchmark scenario F.

$$\begin{aligned}
& + (1 + h_a)(1 - h_b) \left[\frac{\mathcal{Y}}{s^2} + \frac{\mathcal{Z}_2}{s_z^2} + \frac{\mathcal{G}}{s^2} + \frac{\tilde{\mathcal{G}}_{22}}{t_g^2} + \frac{[\mathcal{Y}\mathcal{Z}]_2}{s s_z} + \frac{[\tilde{\mathcal{G}}\mathcal{Y}]_2}{t_g s} + \frac{[\tilde{\mathcal{G}}\mathcal{Z}]_2}{t_g s_z} + \frac{[\tilde{\mathcal{G}}\mathcal{G}]_2}{t_g s} + \sum_{k,l=1,\dots,4} \left(\frac{\mathcal{N}_{22}^{kl}}{t_{\tilde{\chi}_k^0} t_{\tilde{\chi}_l^0}} \right) \right. \\
& + \sum_{k=1,\dots,4} \left(\frac{[\mathcal{N}\mathcal{Y}]_2^k}{t_{\tilde{\chi}_k^0} s} + \frac{[\mathcal{N}\mathcal{Z}]_2^k}{t_{\tilde{\chi}_k^0} s_z} + \frac{[\mathcal{N}\mathcal{G}]_2^k}{t_{\tilde{\chi}_k^0} s} \right) + \sum_{k,l=1,2} \left(\frac{\mathcal{C}_{22}^{kl}}{t_{\tilde{\chi}_k^\pm} t_{\tilde{\chi}_l^\pm}} \right) + \sum_{k=1,2} \left(\frac{[\mathcal{C}\mathcal{Y}]_2^k}{t_{\tilde{\chi}_k^\pm} s} + \frac{[\mathcal{C}\mathcal{Z}]_2^k}{t_{\tilde{\chi}_k^\pm} s_z} + \frac{[\mathcal{C}\mathcal{G}]_2^k}{t_{\tilde{\chi}_k^\pm} s} \right) \Big] \\
& + (1 - h_a)(1 - h_b) \left[\frac{\tilde{\mathcal{G}}_{12}}{t_g^2} + \sum_{k,l=1,\dots,4} \left(\frac{\mathcal{N}_{12}^{kl}}{t_{\tilde{\chi}_k^0} t_{\tilde{\chi}_l^0}} \right) + \sum_{k,l=1,2} \left(\frac{\mathcal{C}_{12}^{kl}}{t_{\tilde{\chi}_k^\pm} t_{\tilde{\chi}_l^\pm}} \right) \right] \\
& + (1 + h_a)(1 + h_b) \left[\frac{\tilde{\mathcal{G}}_{21}}{t_g^2} + \sum_{k,l=1,\dots,4} \left(\frac{\mathcal{N}_{21}^{kl}}{t_{\tilde{\chi}_k^0} t_{\tilde{\chi}_l^0}} \right) + \sum_{k,l=1,2} \left(\frac{\mathcal{C}_{21}^{kl}}{t_{\tilde{\chi}_k^\pm} t_{\tilde{\chi}_l^\pm}} \right) \right], \tag{19}
\end{aligned}$$

where the propagators appear as mass-subtracted Mandelstam variables,

$$s_z = s - m_Z^2, \quad t_{\tilde{\chi}^0} = t - m_{\tilde{\chi}^0}^2, \quad t_{\tilde{\chi}^\pm} = t - m_{\tilde{\chi}^\pm}^2, \quad t_g = t - m_g^2. \tag{20}$$

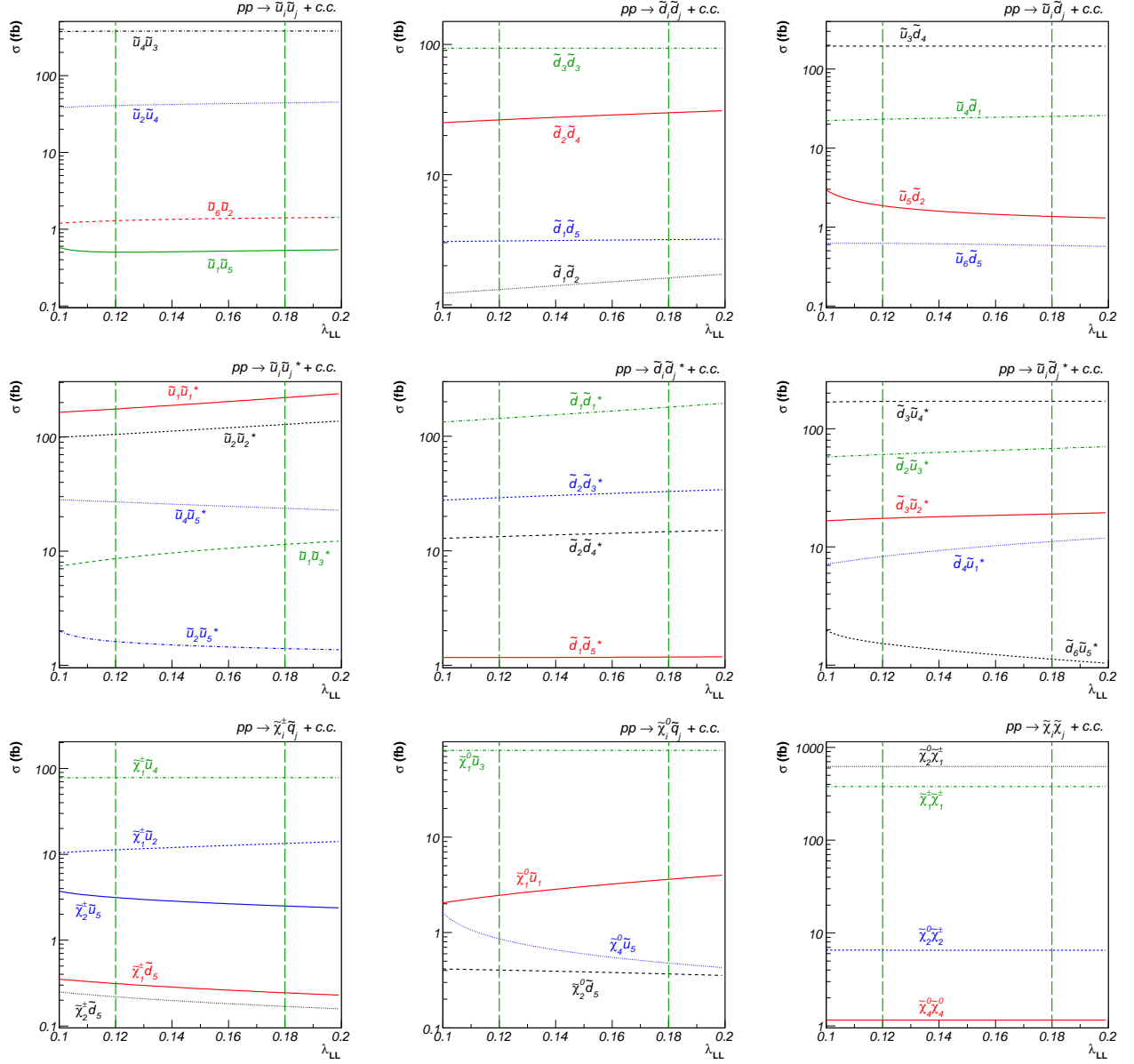


FIG. 19: Same as Fig. 17 for our benchmark scenario F.

Rather compact expressions for the appearing form factors \mathcal{Y} , \mathcal{Z}_m , \mathcal{G} , $[\mathcal{Y}\mathcal{Z}]_m$, $[\tilde{\mathcal{G}}\mathcal{Y}]_m$, $[\tilde{\mathcal{G}}\mathcal{Z}]_m$, $[\tilde{\mathcal{G}}\mathcal{G}]_m$, $[\mathcal{N}\mathcal{Y}]_m^k$, $[\mathcal{N}\mathcal{Z}]_m^k$, $[\mathcal{N}\mathcal{G}]_m^k$, $\tilde{\mathcal{G}}_{nm}$, and \mathcal{N}_{nm}^{kl} ($n, m = 1, 2$ and $k, l = 1, \dots, 4$) and the unchanged gluon-initiated contribution to the cross section are given in Ref. [12]. The additional form factors $[\mathcal{C}\mathcal{Y}]_m^k$, $[\mathcal{C}\mathcal{Z}]_m^k$, $[\mathcal{C}\mathcal{G}]_m^k$, and \mathcal{C}_{nm}^{kl} related to the chargino exchanges read

$$\mathcal{C}_{mn}^{kl} = \frac{\pi \alpha^2}{4 x_W^2 s^2} \mathcal{C}_{\tilde{q}_i q \tilde{\chi}_k^\pm}^{m*} \mathcal{C}_{\tilde{q}_i q \tilde{\chi}_l^\pm}^m \mathcal{C}_{\tilde{q}_j q' \tilde{\chi}_k^\pm}^n \mathcal{C}_{\tilde{q}_j q' \tilde{\chi}_l^\pm}^{n*} \left[\left(u t - m_{\tilde{q}_i}^2 m_{\tilde{q}_j}^2 \right) \delta_{mn} + \left(m_{\tilde{\chi}_k^\pm} m_{\tilde{\chi}_l^\pm} s \right) (1 - \delta_{mn}) \right],$$

$$[\mathcal{C}\mathcal{Y}]_m^k = \frac{\pi \alpha^2 e_q e_{\tilde{q}} \delta_{ij} \delta_{qq'}}{3 x_W s^2} \text{Re} \left[\mathcal{C}_{\tilde{q}_i q \tilde{\chi}_k^\pm}^m \mathcal{C}_{\tilde{q}_j q' \tilde{\chi}_k^\pm}^{m*} \right] \left(u t - m_{\tilde{q}_i}^2 m_{\tilde{q}_j}^2 \right),$$

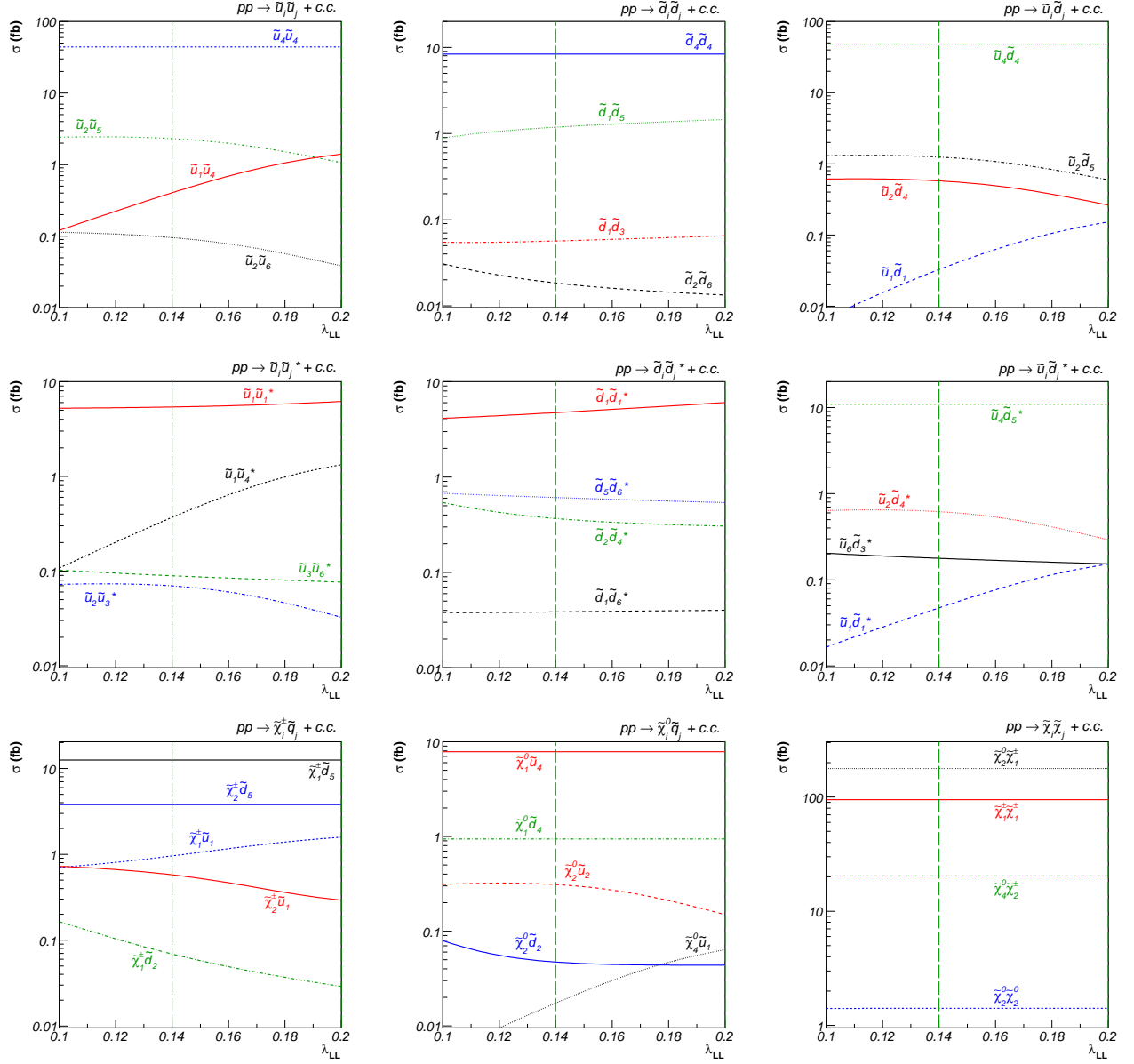


FIG. 20: Same as Fig. 16 for our benchmark scenario G.

$$\begin{aligned}
[\mathcal{CZ}]_m^k &= \frac{\pi \alpha^2}{12 x_W^2 (1 - x_W) s^2} \text{Re} \left[\mathcal{C}_{\tilde{q}_i q \tilde{\chi}_k^\pm}^m \mathcal{C}_{\tilde{q}_j q' \tilde{\chi}_k^\pm}^{m*} (L_{\tilde{q}_i \tilde{q}_j Z} + R_{\tilde{q}_i \tilde{q}_j Z}) \right] \mathcal{C}_{qq'Z}^m \left(u t - m_{\tilde{q}_i}^2 m_{\tilde{q}_j}^2 \right), \\
[\mathcal{CG}]_m^k &= \frac{4 \pi \alpha \alpha_s \delta_{ij} \delta_{qq'}}{9 x_W s^2} \text{Re} \left[\mathcal{C}_{\tilde{q}_i q \tilde{\chi}_k^\pm}^m \mathcal{C}_{\tilde{q}_j q' \tilde{\chi}_k^\pm}^{m*} \right] \left(u t - m_{\tilde{q}_i}^2 m_{\tilde{q}_j}^2 \right)
\end{aligned} \tag{21}$$

with all other variables defined as in Ref. [12]. We take the opportunity to also correct a few minor typographical errors in some of the form factors for the pair production of two up- or down-type squarks (Eq. (36) in Ref. [12])

$$\begin{aligned}
[\mathcal{NTU}]_{mn}^{kl} &= \frac{2 \pi \alpha^2}{3 x_W^2 (1 - x_W)^2 s^2} \text{Re} \left[\mathcal{C}_{\tilde{q}_i q \tilde{\chi}_k^0}^{m*} \mathcal{C}_{\tilde{q}_j q' \tilde{\chi}_k^0}^{n*} \mathcal{C}_{\tilde{q}_i q' \tilde{\chi}_l^0}^n \mathcal{C}_{\tilde{q}_j q \tilde{\chi}_l^0}^m \right] \left[\left(u t - m_{\tilde{q}_i}^2 m_{\tilde{q}_j}^2 \right) (\delta_{mn} - 1) + m_{\tilde{\chi}_k^0} m_{\tilde{\chi}_l^0} s \delta_{mn} \right], \\
[\mathcal{GU}]_{mn} &= \frac{2 \pi \alpha_s^2}{9 s^2} \left| \mathcal{C}_{\tilde{q}_i q' \tilde{g}}^n \mathcal{C}_{\tilde{q}_j q \tilde{g}}^m \right|^2 \left[\left(u t - m_{\tilde{q}_i}^2 m_{\tilde{q}_j}^2 \right) (1 - \delta_{mn}) + m_{\tilde{g}}^2 s \delta_{mn} \right],
\end{aligned}$$

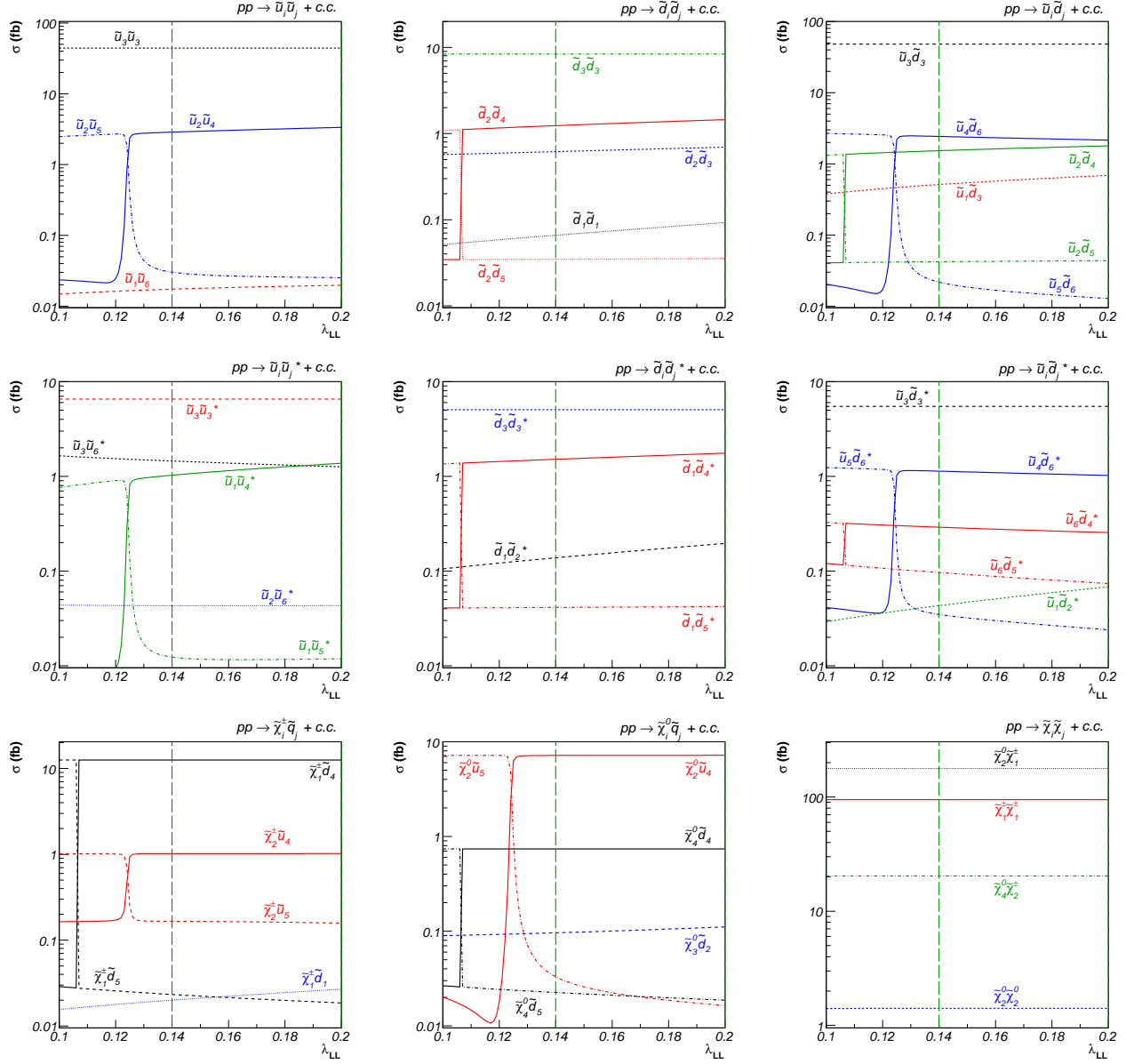


FIG. 21: Same as Fig. 17 for our benchmark scenario G.

$$\begin{aligned}
[\mathcal{GTU}]_{mn} &= \frac{-4\pi\alpha_s^2}{27s^2} \text{Re} \left[\mathcal{C}_{\tilde{q}_i q \tilde{g}}^m \mathcal{C}_{\tilde{q}_j q' \tilde{g}}^n \mathcal{C}_{\tilde{q}_i q' \tilde{g}}^{n*} \mathcal{C}_{\tilde{q}_j q \tilde{g}}^{m*} \right] \left[(ut - m_{\tilde{q}_i}^2 m_{\tilde{q}_j}^2) (\delta_{mn} - 1) + m_{\tilde{g}}^2 s \delta_{mn} \right], \\
[\mathcal{NGA}]_{mn}^k &= \frac{8\pi\alpha\alpha_s}{9s^2 x_W (1 - x_W)} \text{Re} \left[\mathcal{C}_{\tilde{q}_j q' \tilde{\chi}_k^0}^{n*} \mathcal{C}_{\tilde{q}_i q \tilde{\chi}_k^0}^{m*} \mathcal{C}_{\tilde{q}_i q' \tilde{g}}^{n*} \mathcal{C}_{\tilde{q}_j q \tilde{g}}^{m*} \right] \left[(ut - m_{\tilde{q}_i}^2 m_{\tilde{q}_j}^2) (\delta_{mn} - 1) + m_{\tilde{\chi}_k^0} m_{\tilde{g}} s \delta_{mn} \right], \\
[\mathcal{NGB}]_{mn}^k &= \frac{8\pi\alpha\alpha_s}{9s^2 x_W (1 - x_W)} \text{Re} \left[\mathcal{C}_{\tilde{q}_i q' \tilde{\chi}_k^0}^{n*} \mathcal{C}_{\tilde{q}_j q \tilde{\chi}_k^0}^{m*} \mathcal{C}_{\tilde{q}_j q' \tilde{g}}^{n*} \mathcal{C}_{\tilde{q}_i q \tilde{g}}^{m*} \right] \left[(ut - m_{\tilde{q}_i}^2 m_{\tilde{q}_j}^2) (\delta_{mn} - 1) + m_{\tilde{\chi}_k^0} m_{\tilde{g}} s \delta_{mn} \right], \quad (22)
\end{aligned}$$

and in the differential cross section for the production of gaugino pairs (Eq. (40) in Ref. [12])

$$\frac{d\hat{\sigma}_{h_a, h_b}^{q\bar{q}}}{dt} = \frac{\pi\alpha^2}{3s^2} \left[(1 - h_a)(1 + h_b) \left[|Q_{LL}^u|^2 u_{\tilde{\chi}_i} u_{\tilde{\chi}_j} + |Q_{LL}^t|^2 t_{\tilde{\chi}_i} t_{\tilde{\chi}_j} + 2\text{Re}[Q_{LL}^{u*} Q_{LL}^t] m_{\tilde{\chi}_i} m_{\tilde{\chi}_j} s \right] \right]$$

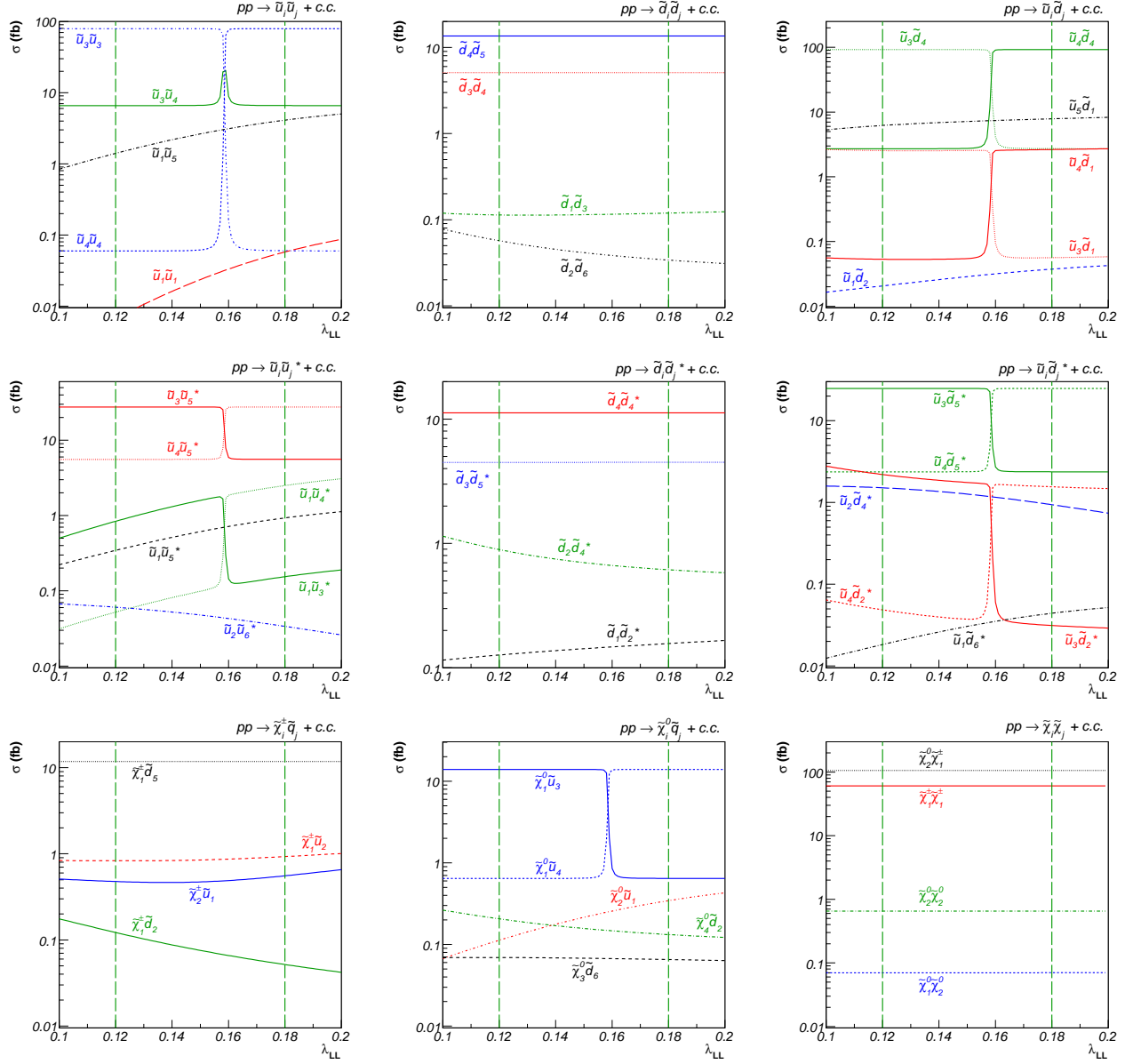


FIG. 22: Same as Fig. 16 for our benchmark scenario H.

$$\begin{aligned}
& + (1 + h_a)(1 - h_b) \left[|Q_{RR}^u|^2 u_{\tilde{\chi}_i} u_{\tilde{\chi}_j} + |Q_{RR}^t|^2 t_{\tilde{\chi}_i} t_{\tilde{\chi}_j} + 2\text{Re}[Q_{RR}^{u*} Q_{RR}^t] m_{\tilde{\chi}_i} m_{\tilde{\chi}_j} s \right] \\
& + (1 + h_a)(1 + h_b) \left[|Q_{RL}^u|^2 u_{\tilde{\chi}_i} u_{\tilde{\chi}_j} + |Q_{RL}^t|^2 t_{\tilde{\chi}_i} t_{\tilde{\chi}_j} + 2\text{Re}[Q_{RL}^{u*} Q_{RL}^t] (ut - m_{\tilde{\chi}_i}^2 m_{\tilde{\chi}_j}^2) \right] \\
& + (1 - h_a)(1 - h_b) \left[|Q_{LR}^u|^2 u_{\tilde{\chi}_i} u_{\tilde{\chi}_j} + |Q_{LR}^t|^2 t_{\tilde{\chi}_i} t_{\tilde{\chi}_j} + 2\text{Re}[Q_{LR}^{u*} Q_{LR}^t] (ut - m_{\tilde{\chi}_i}^2 m_{\tilde{\chi}_j}^2) \right].
\end{aligned} \tag{23}$$

In Figs. 16 – 27, we show examples of the obtained numerical cross sections for charged squark-squark pair production, neutral and charged squark-antisquark pair production, associated production of squarks with charginos and neutralinos, and gaugino-pair production at the LHC for our benchmark points E, F, G, H, I, and J and for both of the two considered implementations of non-minimal flavour violation in the GMSB model discussed in Sec. II. We recall that the first is based on mixing between matter and fundamental messengers, leading to flavour mixing only in the left-left chiral squark sector and implemented at the electroweak scale through the parameter λ_{LL} , while λ_{RR} is set to zero. The second scenario involves mixing with antisymmetric messengers, giving rise to flavour violation in both the left-left and right-right chiral squark sectors governed by the parameter $\lambda_{LL} = \lambda_{RR}$. For the sake of better

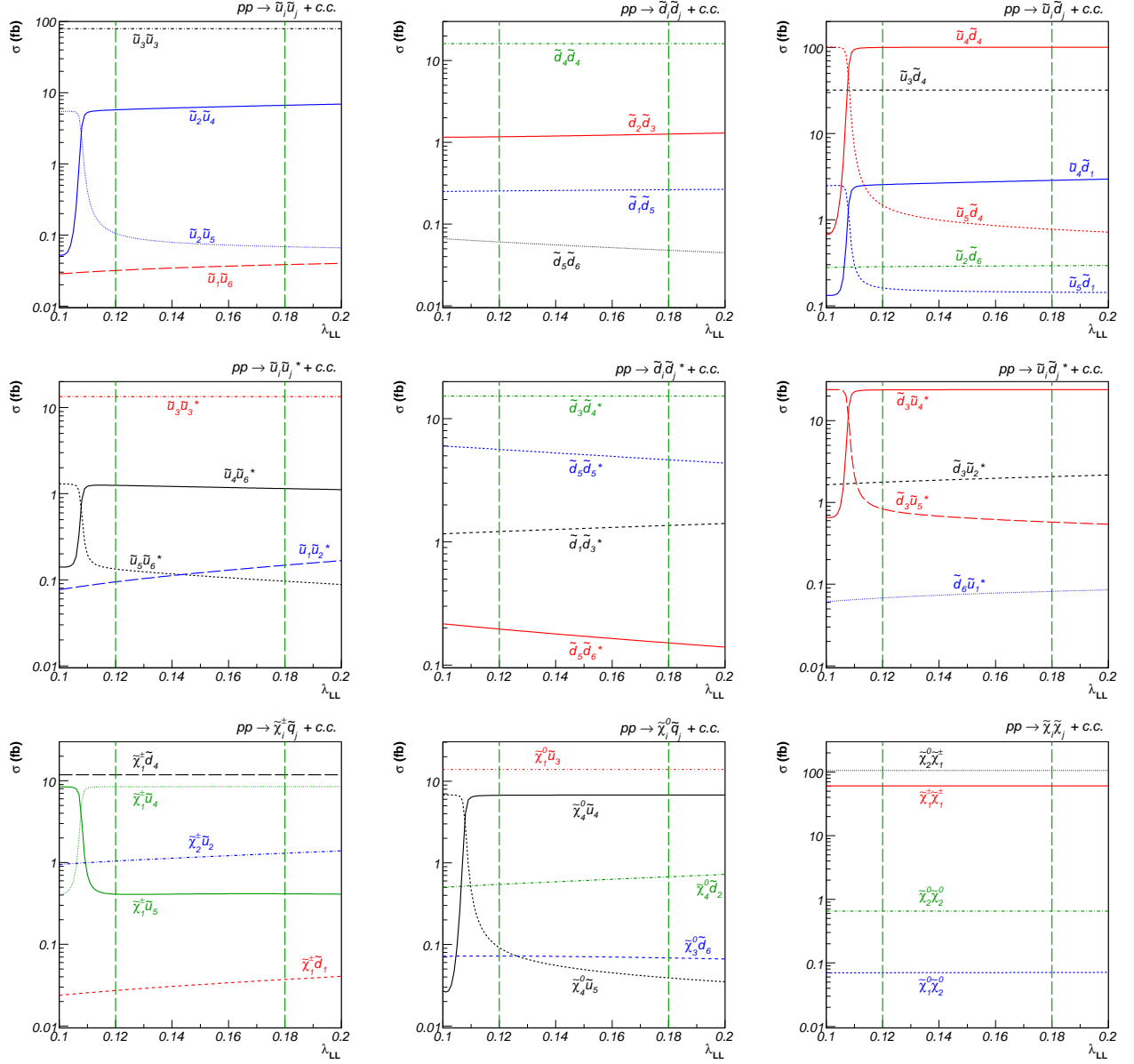


FIG. 23: Same as Fig. 17 for our benchmark scenario H.

readability, we show only the numerically most important curves as well as a selection of those that involve visible flavour-violating effects.

The magnitudes of the cross sections vary from the barely visible level of 10^{-2} fb for weak production of heavy final states over the semi-strong production of average squarks and gauginos and quark-gluon initial states to large cross sections of 10^2 to 10^3 fb for the strong production of diagonal squark-squark and squark-antisquark pairs or weak production of very light gaugino pairs. Unfortunately, the processes whose cross sections are largest are mostly insensitive to the parameter λ_{LL} in both flavour violation scenarios, as the strong gauge interaction is insensitive to quark flavours and gaugino pair production cross sections are summed over exchanged squark flavours.

Some of the subleading, non-diagonal cross sections show, however, sharp transitions in particular squark production channels. These transitions are directly related to the “avoided crossings” of the mass eigenvalues discussed in Sec. III. At the point, where two levels should cross, the involved squarks change character and are subject to an exchange of their flavour contents. Rather than the mass dependence on λ_{LL} , these exchanges then lead, together with the different parton densities in the proton, to more or less sharp transitions in the production cross sections, where the corresponding squarks are involved. This phenomenon is analogously observed in the case of squark and gaugino hadroproduction in minimal supergravity [12].

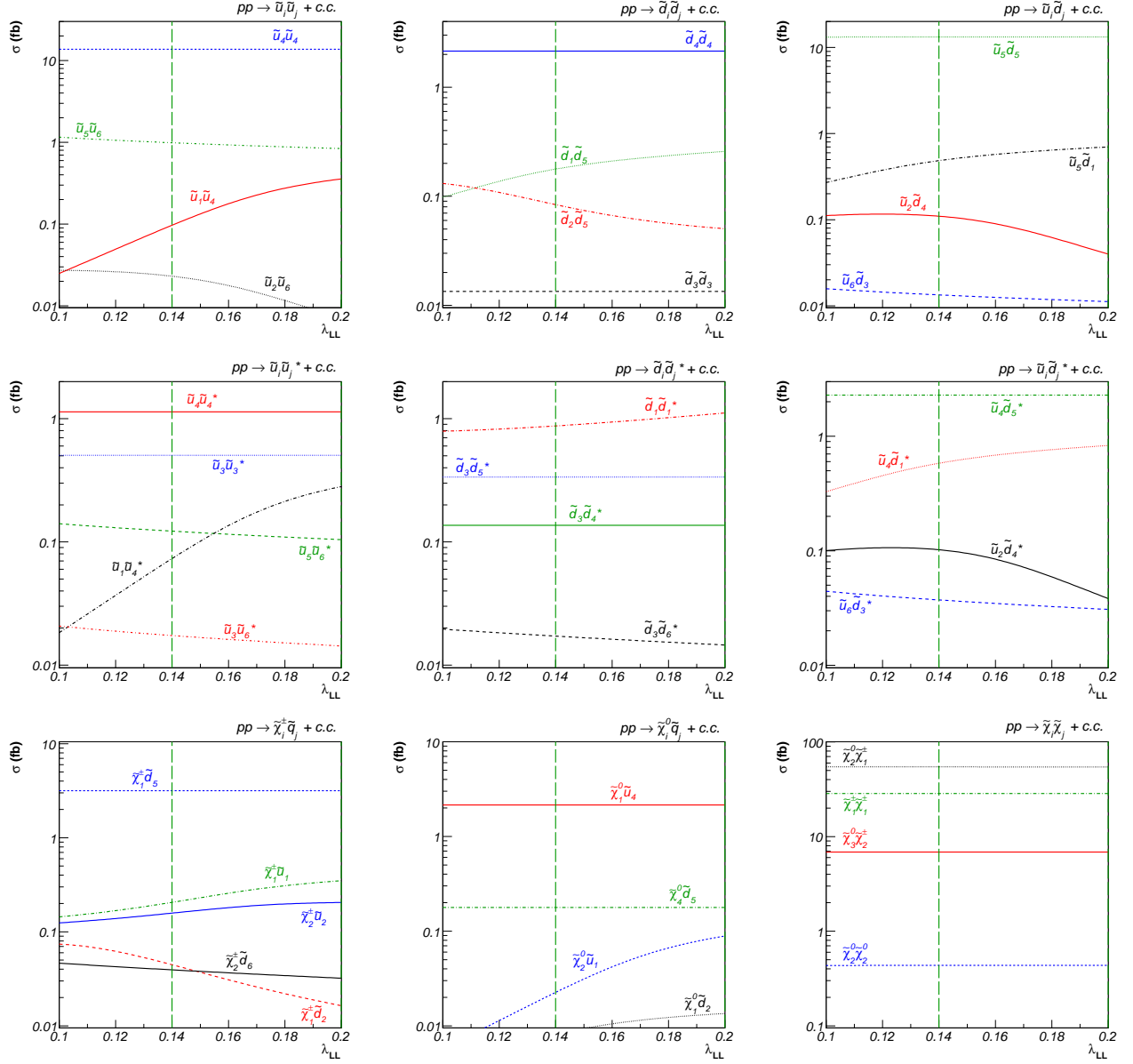


FIG. 24: Same as Fig. 16 for our benchmark scenario I.

As an example, let us discuss in detail the production of squarks and gauginos for our benchmark point E. The cross sections in our flavour violation scenario based on fundamental messengers are shown in Fig. 16. “Avoided crossings” of mass eigenvalues occur here, e.g., for down-type squarks at a value of $\lambda_{LL} \approx 0.145$ between the squarks \tilde{d}_3 and \tilde{d}_4 , see also Fig. 8. Before this point, \tilde{d}_3 is characterized by a dominant sdown content, while \tilde{d}_4 has first a dominant sbottom and then sstrange content. For $\lambda_{LL} \gtrsim 0.145$, these contents are exchanged, i.e. \tilde{d}_3 is then a strange-squark and \tilde{d}_4 becomes sdown-like. As a consequence, the cross sections involving the two mass eigenstates exchange their values, since the production of first generation squarks is preferred due to the more important parton density of up- and down-type quarks in the proton. This can be seen in our example for the production of down-type squark-squark and squark-antisquark pairs, mixed up- and down-type squark-squark and squark-antisquark pair production, as well as for the associated production of down-type squarks and charginos or neutralinos. For up-type squarks, the level-reordering phenomenon occurs at values of $\lambda_{LL} \simeq 0.09$ in the range excluded by $\text{BR}(b \rightarrow s\gamma)$ (left of the vertical dashed/green line) and is therefore not shown here. However, another effect becomes visible in the case of production cross sections that involve final states with up-type squarks. Some of the mass eigenstates do not present sharp transitions, but rather a continuous change in their flavour content. This is, e.g., the case for the lightest mass eigenstate \tilde{u}_1 . The corresponding production cross sections increase smoothly with the flavour violation parameter

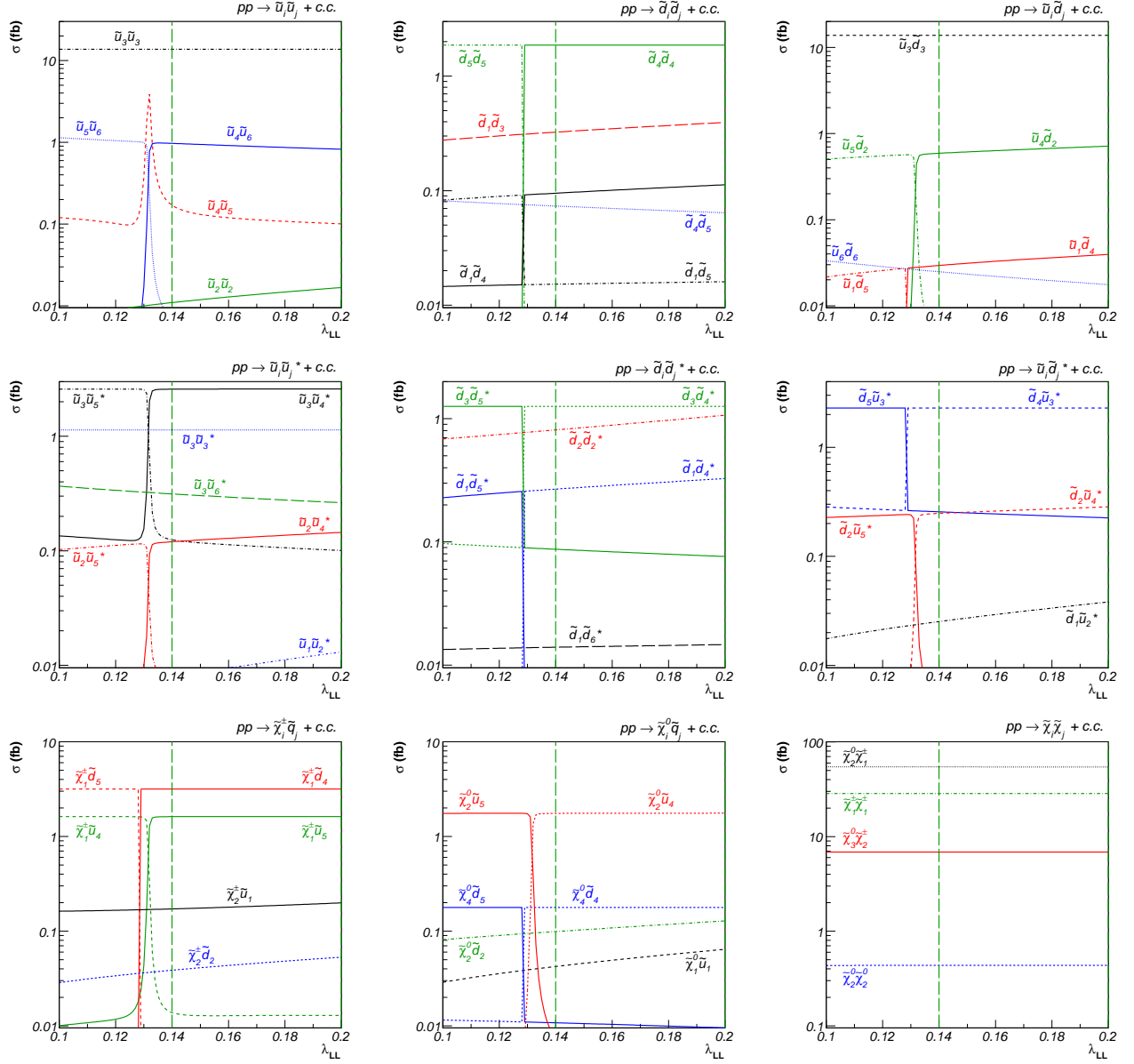


FIG. 25: Same as Fig. 17 for our benchmark scenario I.

λ_{LL} , which is explained by the fact that for lower values of λ_{LL} the lightest up-type squark \tilde{u}_1 is mostly stop-like, but receives sizable contributions of the light flavours for higher λ_{LL} . Together with the more important parton densities, this results in an increase of the corresponding production cross sections. In the same way, we also observe cross sections that decrease with λ_{LL} , due to a decrease of their light flavour content.

The same phenomena are observed in the case of our second flavour violation scenario with antisymmetric messengers, see Fig. 17 for the benchmark point E. Note that here also “avoided crossings” between up-type squark mass eigenstates are observed, e.g. between \tilde{u}_4 and \tilde{u}_5 at $\lambda_{LL} \approx 0.11$, which lies, however, already in the range excluded by $\text{BR}(b \rightarrow s\gamma)$. In this example, the \tilde{u}_5 loses its important up-squark content to the scharm-dominated \tilde{u}_4 . The latter becomes then purely sup-like, enhancing its production cross section due to the parton density in the proton, while the cross sections involving \tilde{u}_5 become less important.

For the benchmark points H with fundamental (Fig. 22) and I (Fig. 25) and J (Fig. 27) with antisymmetric messengers, we observe a third effect at $\lambda_{LL} = 0.158, 0.132$ and 0.114 , respectively. Here, the pair production of up-type squark pairs ($\tilde{u}_3\tilde{u}_4$ for fundamental and $\tilde{u}_4\tilde{u}_5$ for antisymmetric messengers) exhibits an interesting resonance-like behaviour. It is generated by the fact that these squark mass eigenstates exchange their up and charm flavour contents (and also their chiralities in the case of antisymmetric messengers) at the critical λ_{LL} -values in a rather smooth way,

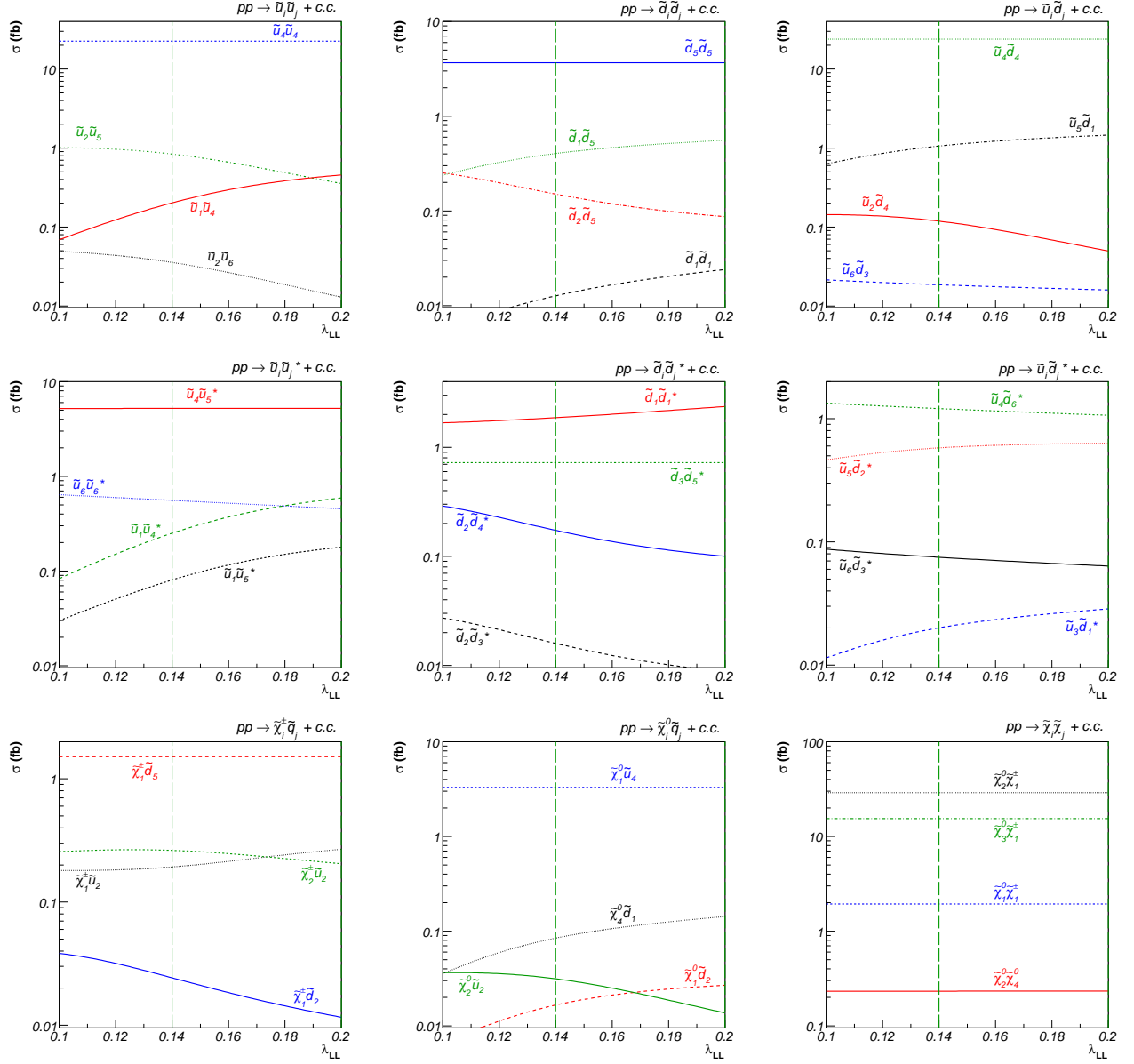


FIG. 26: Same as Fig. 16 for our benchmark scenario J.

so that both squark mass eigenstates receive significant up- (valence-) quark contributions to their production cross sections in the vicinity.

We remind the reader that in the case of flavour mixing only in the left-left chiral sector, “avoided crossings” occur among the $\tilde{q}_{1,2}$, $\tilde{q}_{3,4}$, and $\tilde{q}_{5,6}$ mass eigenstates, whereas in the case of flavour mixing in both the left-left and right-right chiral squark sectors, we rather observe the mass flips among the $\tilde{q}_{2,3}$ and $\tilde{q}_{4,5}$ mass eigenstates, respectively. Note also that the difference between the two flavour violation scenarios is invisible for the gaugino pair production in the bottom right panels of Figs. 16 – 27, respectively, that are practically insensitive to flavour violation in the squark sector.

Concerning the production of gravitinos, the cross sections achieve sizable orders of magnitude only in the case of a rather light gravitino, see e.g. Ref. [14]. If the latter is too heavy, its couplings are too small to yield discoverable cross sections, since they are proportional to the inverse of the gravitino mass squared. In particular, this is the case for our scenarios with gravitino cold dark matter, where we have found a value of the order of $m_{\tilde{G}} \sim 10^{-1}$ GeV derived from the different cosmological constraints. Note that in order to have a very light gravitino and consequently sizable production cross sections, one could consider a GMSB scenario with gravitino hot dark matter ($m_{\tilde{G}} \lesssim 1$ keV) and additional cold dark matter from stable messenger particles [43–46]. In scenarios with a mixing between messenger

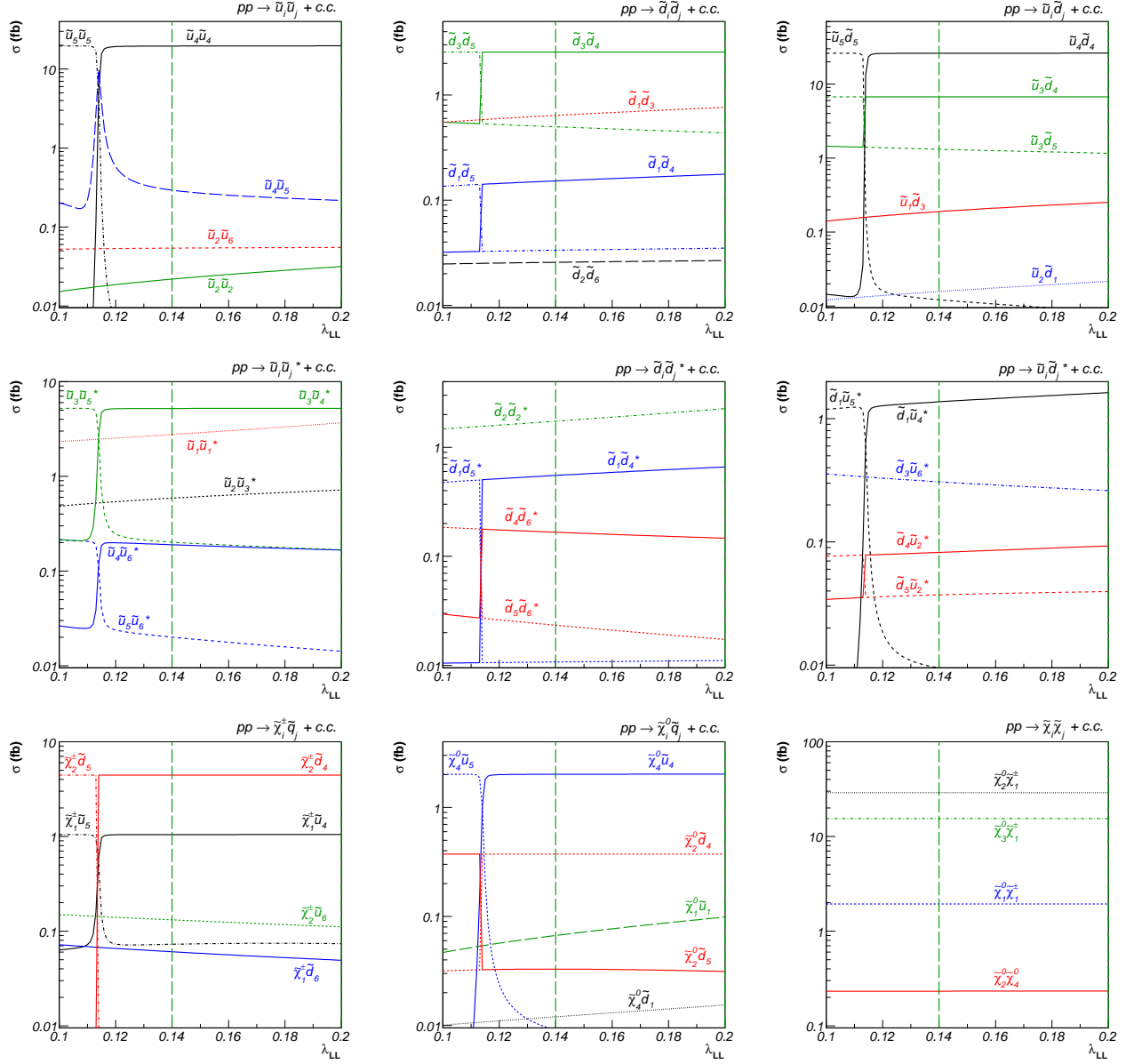


FIG. 27: Same as Fig. 17 for our benchmark scenario J.

and matter fields, however, the stability of the lightest messenger might be lost. We therefore do not consider the production of light gravitinos in our GMSB scenarios with additional flavour violation in the squark sector.

VI. CONCLUSIONS

While SUSY-breaking mediated by gauge interactions may be in principle attractive, since the gauge interactions do not induce flavour violation as do the gravitational interactions, the parameter space of minimal GMSB models is today severely constrained by low-energy, electroweak precision, and cosmological constraints, in particular from the flavour-changing neutral-current decay $b \rightarrow s\gamma$.

We have discussed several possibilities how flavour violation may still be induced in GMSB models. Focusing on messenger-matter mixing scenarios with fundamental or antisymmetric messengers and flavour violation in the left-left only or left-left and right-right chiral squark sectors, we have established collider-friendly regions of parameter space that are at the same time cosmologically viable and allow for the definition of benchmark points with neutralino or stau NLSPs.

Depending on the strength of the flavour-violating parameter λ_{LL} , we showed that splittings and avoided crossings appear in the mass spectra, inducing at the same time smooth or sharp transitions in the squark flavour contents. This induces interesting phenomenological consequences, in particular for squark and gaugino production cross sections at the LHC induced by valence and sea quark parton densities that differ largely in magnitude.

We had hoped to also be able to investigate gravitino production and decay with flavour violation at the LHC. This was, however, not possible, since cosmological constraints require either a relatively heavy gravitino as a CDM candidate, with masses of 10^{-4} – 10^{-1} GeV and consequently unobservably small cross sections, or additional messenger dark matter, which would have been incompatible with our messenger-matter mixing scenario.

Acknowledgments

The authors would like to thank L. Covi, G. Hiller, W. Hollik, S. Kraml and F.D. Steffen for useful discussions. This work was supported by a Ph.D. fellowship of the French ministry for education and research and by the *Theory LHC France* initiative of CNRS-IN2P3.

-
- [1] H. P. Nilles, Phys. Rept. **110** (1984) 1.
 - [2] H. E. Haber and G. L. Kane, Phys. Rept. **117** (1985) 75.
 - [3] M. Dine, W. Fischler and M. Srednicki, Nucl. Phys. B **189** (1981) 575;
S. Dimopoulos and S. Raby, Nucl. Phys. B **192** (1982) 353;
C. Nappi and B. Ovrut, Phys. Lett. B **113** (1982) 175.
 - [4] M. Dine and A. E. Nelson, Phys. Rev. D **48** (1993) 1277;
M. Dine, A. E. Nelson and Y. Shirman, Phys. Rev. D **51** (1995) 1362;
M. Dine, A. E. Nelson, Y. Nir and Y. Shirman, Phys. Rev. D **53** (1996) 2658.
 - [5] G. F. Giudice and R. Rattazzi, Nucl. Phys. B **511** (1998) 25;
N. Arkani-Hamed, G. F. Giudice, M. A. Luty and R. Rattazzi, Phys. Rev. D **58** (1998) 115005.
 - [6] G. F. Giudice and R. Rattazzi, Phys. Rept. **322** (1999) 419.
 - [7] K. Tobe, J. D. Wells and T. Yanagida, Phys. Rev. D **69** (2004) 035010.
 - [8] S. L. Dubovsky and D. S. Gorbunov, Nucl. Phys. B **557** (1999) 119.
 - [9] J. S. Hagelin, S. Kelley and T. Tanaka, Nucl. Phys. B **415** (1994) 293.
 - [10] F. Gabbiani, E. Gabrielli, A. Masiero and L. Silvestrini, Nucl. Phys. B **477** (1996) 321.
 - [11] M. Ciuchini, A. Masiero, P. Paradisi, L. Silvestrini, S. K. Vempati and O. Vives, Nucl. Phys. B **783** (2007) 112.
 - [12] G. Bozzi, B. Fuks, B. Herrmann and M. Klasen, Nucl. Phys. B **787** (2007) 1.
 - [13] W. M. Yao *et al.* [Particle Data Group], J. Phys. G **33** (2006) 1, and 2007 partial update.
 - [14] M. Klasen and G. Pignol, Phys. Rev. D **75** (2007) 115003.
 - [15] E. Barberio *et al.* [Heavy Flavor Averaging Group (HFAG)], hep-ex/0603003.
 - [16] T. Hahn, W. Hollik, J. I. Illana and S. Penaranda, hep-ph/0512315.
 - [17] A. L. Kagan and M. Neubert, Phys. Rev. D **58** (1998) 094012.
 - [18] S. Heinemeyer, W. Hollik, F. Merz and S. Penaranda, Eur. Phys. J. C **37** (2004) 481.
 - [19] S. Heinemeyer, D. Stöckinger and G. Weiglein, Nucl. Phys. B **690** (2004) 62.
 - [20] S. Heinemeyer, D. Stöckinger and G. Weiglein, Nucl. Phys. B **699** (2004) 103.
 - [21] T. Moroi, Phys. Rev. D **53** (1996) 6565 [Erratum-ibid. D **56** (1997) 4424].
 - [22] W. Porod, Comput. Phys. Commun. **153** (2003) 275.
 - [23] S. Heinemeyer, W. Hollik and G. Weiglein, Comput. Phys. Commun. **124** (2000) 76.
 - [24] B. C. Allanach *et al.*, Eur. Phys. J. C **25** (2002) 113.
 - [25] S. Heinemeyer, X. Miao, S. Su and G. Weiglein, arXiv:0805.2359 [hep-ph].
 - [26] F. del Aguila *et al.*, arXiv:0801.1800 [hep-ph].
 - [27] J. Foster, K. I. Okumura and L. Roszkowski, Phys. Lett. B **641** (2006) 452.
 - [28] S. Dittmaier, G. Hiller, T. Plehn and M. Spannowsky, Phys. Rev. D **77** (2008) 115001.
 - [29] P. Gambino, U. Haisch and M. Misiak, Phys. Rev. Lett. **94** (2005) 061803.
 - [30] H. Goldberg, Phys. Rev. Lett. **50** (1983) 1419.
 - [31] J. R. Ellis, J. S. Hagelin, D. V. Nanopoulos, K. A. Olive and M. Srednicki, Nucl. Phys. B **238** (1984) 453.
 - [32] J. Hamann, S. Hannestad, M. S. Sloth and Y. Y. Y. Wong, Phys. Rev. D **75** (2007) 023522.
 - [33] J. R. Ellis, K. A. Olive, Y. Santoso and V. C. Spanos, Phys. Lett. B **565** (2003) 176.
 - [34] M. Bolz, A. Brandenburg and W. Buchmüller, Nucl. Phys. B **606** (2001) 518, [Erratum-ibid. B **790** (2008) 336].
 - [35] J. Pradler and F. D. Steffen, Phys. Rev. D **75** (2007) 023509.
 - [36] V. S. Rychkov and A. Strumia, Phys. Rev. D **75** (2007) 075011.
 - [37] W. Buchmüller, P. Di Bari and M. Plümacher, Annals Phys. **315** (2005) 305.
 - [38] J. Pradler and F. D. Steffen, Phys. Lett. B **648** (2007) 224.

- [39] G. Bélanger, F. Boudjema, A. Pukhov and A. Semenov, *Comput. Phys. Commun.* **149** (2002) 103.
- [40] P. Gondolo, J. Edsjo, P. Ullio, L. Bergstrom, M. Schelke and E. A. Baltz, *JCAP* **0407** (2004) 008.
- [41] M. Pospelov, J. Pradler and F. D. Steffen, arXiv:0807.4287 [hep-ph].
- [42] J. Pumplin, D. R. Stump, J. Huston, H. L. Lai, P. Nadolsky and W. K. Tung, *JHEP* **0207** (2002) 012.
- [43] T. Falk, K. A. Olive and M. Srednicki, *Phys. Lett. B* **339** (1994) 248.
- [44] S. Dimopoulos, G. F. Giudice and A. Pomarol, *Phys. Lett. B* **389** (1996) 37.
- [45] D. Hooper and J. March-Russell, *Phys. Lett. B* **608** (2005) 17.
- [46] M. Ibe, K. Tobe and T. Yanagida, *Phys. Lett. B* **615** (2005) 120.